NAVAL POSTGRADUATE SCHOOL

MONTEREY, CALIFORNIA

THESIS

MODELING OF RADIOWAVE PROPAGATION IN A FORESTED ENVIRONMENT

by

Yeow Chong Daniel Ng

September 2014

Thesis Advisor:	David C. Jenn
Second Reader:	Phillip E. Pace

Approved for public release; distribution is unlimited

THIS PAGE INTENTIONALLY LEFT BLANK

REPORT DOCUMENTATION PAGE

Form Approved OMB No. 0704–0188

1. AGENCY USE ONLY *(Leave blank)*	**2. REPORT DATE** September 2014	**3. REPORT TYPE AND DATES COVERED** Master's Thesis

4. TITLE AND SUBTITLE
MODELING OF RADIOWAVE PROPAGATION IN A FORESTED ENVIRONMENT

5. FUNDING NUMBERS

6. AUTHOR(S) Yeow Chong Daniel Ng

7. PERFORMING ORGANIZATION NAME(S) AND ADDRESS(ES)
Naval Postgraduate School
Monterey, CA 93943-5000

8. PERFORMING ORGANIZATION REPORT NUMBER

9. SPONSORING /MONITORING AGENCY NAME(S) AND ADDRESS(ES)
N/A

10. SPONSORING/MONITORING AGENCY REPORT NUMBER

11. SUPPLEMENTARY NOTES The views expressed in this thesis are those of the author and do not reflect the official policy or position of the Department of Defense or the U.S. Government. IRB Protocol number ____N/A____.

12a. DISTRIBUTION / AVAILABILITY STATEMENT
Approved for public release; distribution is unlimited

12b. DISTRIBUTION CODE

13. ABSTRACT (maximum 200 words)

Propagation models used in wireless communication system design play an important role in overall link performance. Propagation models in a forested environment, in particular, are especially valuable and complex due to the randomly distributed leaves, twigs, trunks, and trees. This has been an area of interest due to the operational needs of military and non-military domains. Applications in both domains require communication devices and sensors to be operated in forested environments.

Various methods have been employed to model propagation loss. There are experimental measurements, empirical models, analytical, and computational electromagnetic methods. Each method has its applicability and limitations. In this thesis, investigation of a three-layer homogenous medium model (air, forest, and ground) by a ray tracing method was carried out. Both transmitting antenna and observation point are within the forest layer.

The results from the ray tracing model showed good agreement with the available measurement data up to 100 MHz. Further, better approximation of the transmission loss was observed at separation distances greater than 1 km. Values of the effective electrical properties of the forest played an important role in transmission loss estimation within the forest. After adjustment, the deviation in propagation loss using the ray tracing model achieved an error of ± 1 dB.

14. SUBJECT TERMS Ray tracing method, three-layer homogeneous medium model, propagation loss, forested environment	**15. NUMBER OF PAGES** 85
	16. PRICE CODE

17. SECURITY CLASSIFICATION OF REPORT	**18. SECURITY CLASSIFICATION OF THIS PAGE**	**19. SECURITY CLASSIFICATION OF ABSTRACT**	**20. LIMITATION OF ABSTRACT**
Unclassified	Unclassified	Unclassified	UU

NSN 7540–01-280-5500

Standard Form 298 (Rev. 2–89)
Prescribed by ANSI Std. 239–18

THIS PAGE INTENTIONALLY LEFT BLANK

Approved for public release; distribution is unlimited

MODELING OF RADIOWAVE PROPAGATION IN A FORESTED ENVIRONMENT

Yeow Chong Daniel Ng
Civilian, ST Electronics, Singapore
B.S., Nanyang Technological University, 2006

Submitted in partial fulfillment of the
requirements for the degree of

MASTER OF SCIENCE IN ELECTRICAL ENGINEERING

from the

NAVAL POSTGRADUATE SCHOOL
September 2014

Author: Yeow Chong Daniel Ng

Approved by: David C. Jenn
Thesis Advisor

Phillip E. Pace
Second Reader

R. Clark Robertson
Chair, Department of Electrical and Computer Engineering

THIS PAGE INTENTIONALLY LEFT BLANK

ABSTRACT

Propagation models used in wireless communication system design play an important role in overall link performance. Propagation models in a forested environment, in particular, are especially valuable and complex due to the randomly distributed leaves, twigs, trunks, and trees. This has been an area of interest due to the operational needs of military and non-military domains. Applications in both domains require communication devices and sensors to be operated in forested environments.

Various methods have been employed to model propagation loss. There are experimental measurements, empirical models, analytical, and computational electromagnetic methods. Each method has its applicability and limitations. In this thesis, investigation of a three-layer homogenous medium model (air, forest, and ground) by a ray tracing method was carried out. Both transmitting antenna and observation point are within the forest layer.

The results from the ray tracing model showed good agreement with the available measurement data up to 100 MHz. Further, better approximation of the transmission loss was observed at separation distances greater than 1 km. Values of the effective electrical properties of the forest played an important role in transmission loss estimation within the forest. After adjustment, the deviation in propagation loss using the ray tracing model achieved an error of $\pm$ 1 dB.

THIS PAGE INTENTIONALLY LEFT BLANK

TABLE OF CONTENTS

I. INTRODUCTION....1
A. RADIOWAVE PROPAGATION IN A FORESTED ENVIRONMENT....1
B. BACKGROUND....2
C. THESIS OBJECTIVE....4
D. THESIS OUTLINE....5

II. METHODOLOGY USED FOR MODELING....7
A. ANALYTICAL METHODS....7
B. EM PLANE WAVE PROPAGATION....10
C. ELECTRICAL PROPERTIES OF THE MEDIA....14
D. ELECTROMAGNETIC WAVE PROPAGATION MECHANISM FOR FOREST LAYER....15
E. EMPIRICAL MODELS....16

III. RAY TRACING MODEL....23
A. ASSUMPTIONS AND CONSIDERATIONS....24
B. MODEL FORMULATIONS....24
1. Propagation Constant....25
2. Path Length Computation....25
3. Geometrical Optics Waves Formulation....28
4. Antenna Pattern Factor....28
5. Lateral Wave Formulation....31
6. Transmission Loss Definition....32

IV. RESULTS AND ANALYSIS....33
A. CASE I SETUP AND SIMULATION....33
1. Case I Results....35
2. Case I Analysis and Comments....39
B. CASE II SETUP AND SIMULATION....40
1. Case II Results....41
2. Case II Analysis and Comments....43

V. CONCLUSIONS AND RECOMMENDATIONS....45
A. SUMMARY....45
B. CONCLUSION....46
C. RECOMMENDATIONS....47

APPENDIX A. SOFTWARE DESCRIPTION....49

APPENDIX B. ABSOLUTE DIFFERENCE DATA FOR CASE I....53

APPENDIX C. ABSOLUTE DIFFERENCE DATA FOR CASE II....55

LIST OF REFERENCES....57

INITIAL DISTRIBUTION LIST....61

THIS PAGE INTENTIONALLY LEFT BLANK

LIST OF FIGURES

Figure 1. Layered model of the rain forest (after [2], [3]).....1
Figure 2. Illustration of propagation mechanisms (after [12]).....4
Figure 3. Various configurations for deterministic modeling (after [18]).....7
Figure 4. EM wave propagating in positive $\hat{z}$-direction.....10
Figure 5. Polarization for electric field vector (after [27]).....13
Figure 6. Ray tracing model.....23
Figure 7. Four possible cases for the path length computation.....26
Figure 8. E - plane and H - plane radiation plots for an ideal dipole (after [33]).....29
Figure 9. Geometry setup for antenna factor analysis.....30
Figure 10. Effect of the antenna element factor on direct and reflected E field at 100 MHz.....30
Figure 11. Reference electric field for computing the transmission loss.....32
Figure 12. Measured data from [14] versus ray tracing model (1.6 km, 25 MHz, V-pol).....36
Figure 13. Measured data from [14] versus ray tracing model (1.6 km, 50 MHz, V-pol).....37
Figure 14. Measured data from [14] versus ray tracing model (1.6 km, 100 MHz, V-pol).....37
Figure 15. Measured data from [14] versus ray tracing model (1.6 km, 25 MHz, H-pol).....38
Figure 16. Measured data from [14] versus ray tracing model (1.6 km, 50 MHz, H-pol).....38
Figure 17. Measured data from [14] versus ray tracing model (1.6 km, 100 MHz, H-pol).....39
Figure 18. Measured data from [7] versus predictions from models at 50 MHz, V-pol…41
Figure 19. Measured data from [7] versus prediction from models at 50 MHz, H-pol. ...42
Figure 20. Overview of ray tracing model in MATLAB simulation environment.....50
Figure 21. Generic flow diagram within Block A.....50
Figure 22. Generic flow diagram within Block B.....51

THIS PAGE INTENTIONALLY LEFT BLANK

LIST OF TABLES

Table 1. Summary table for the various analytic methods used to model propagation loss. 9
Table 2. Electrical properties of forest medium (after [26]). 15
Table 3. Constants for the JB Model (after [10]). 19
Table 4. Constants for the Tewari's empirical model (after [7]). 20
Table 5. Geometrical inputs for Case I. 33
Table 6. Initial electrical properties of media for Case I. 34
Table 7. Effective permittivity and conductivity for the ray tracing method and Sommerfeld solution from [14] (V-pol). 35
Table 8. Effective permittivity and conductivity for the ray tracing method and Sommerfeld solution from [14] (H-pol). 36
Table 9. Average error between measured data from [14] and ray tracing model with adjusted parameter. 40
Table 10. Geometrical inputs for Case II. 40
Table 11. Electrical properties of each medium for Case II. 41
Table 12. RMS error at 50 MHz. 42
Table 13. RMS error at 50 MHz with D greater than 1.0 km. 43
Table 14. RMS error with D greater than 1.0 km and lower forest conductivity. 44
Table 15. Input parameters for the ray tracing model. 49
Table 16. Absolute difference (dB) between ray tracing model and measured data at 25 MHz (V-pol). 53
Table 17. Absolute difference (dB) between ray tracing model and measured data at 50 MHz (V-pol). 53
Table 18. Absolute difference (dB) between ray tracing model and measured data at 100 MHz (V-pol). 53
Table 19. Absolute difference (dB) between ray tracing model and measured data at 25 MHz (H-pol). 54
Table 20. Absolute difference (dB) between ray tracing model and measured data at 50 MHz (H-pol). 54
Table 21. Absolute difference (dB) between ray tracing model and measured data at 100 MHz (H-pol). 54
Table 22. Absolute difference (dB) between ray tracing model and measured data at 50 MHz (V-pol). 55
Table 23. Absolute difference (dB) between ray tracing model and measured data at 50 MHz (H-pol). 55

THIS PAGE INTENTIONALLY LEFT BLANK

LIST OF ACRONYMS AND ABBREVIATIONS

CEM	Computational Electromagnetic Method
CST	Computer Simulation Technology
EM	electromagnetic
GO	Geometrical Optics
H-pol	Horizontal Polarization
ITU-R	International Telecommunication Union Recommendation
JB	Jansky and Bailey
LITU-R	Lateral ITU-R
MED	Modified Exponential Decay
MWS	Microwave Studio
OWLs	Open-wire transmission lines
PE	Parabolic Equation
RMS	root mean square
Rx	receiving
Tx	transmitting
UAV	unmanned aerial vehicle
UGS	unmanned ground sensor
UHF	ultra high frequency
VHF	very high frequency
V-pol	Vertical Polarization

THIS PAGE INTENTIONALLY LEFT BLANK

EXECUTIVE SUMMARY

Many applications, both in the military and non-military domains, require the use of communication links within or through foliage. Examples of military applications are the communication link between dismounted soldiers and the central node within the forested environment, unmanned ground sensors (UGS) deployed in a forested environment, and downlink communication from an unmanned aerial vehicle (UAV) to troops located within a forest. Other non-military applications are remote sensor networks for agriculture monitoring of farming operations and search and rescue missions in a forested environment. These real-world applications stimulate the need for radiowave propagation studies in foliage.

In an actual forest environment, tree trunks and leaves are randomly distributed. This randomness causes attenuation, scattering, diffraction, and absorption of the signal energy. Such characteristics make the modeling of the foliage environment a complex problem. Moreover, there are various types of woodlands and each has characteristics that are different depending on the climate. The classification of different layers within the forest is shown in Figure 1. This classification of layers provides a simplified model for analyzing the problem [1]. If the variation within each level as a function of distance is small compared to the wavelength of the propagating wave, an effective homogeneous medium can be defined for each layer. The electrical parameters that define the media are their permittivity and conductivity.

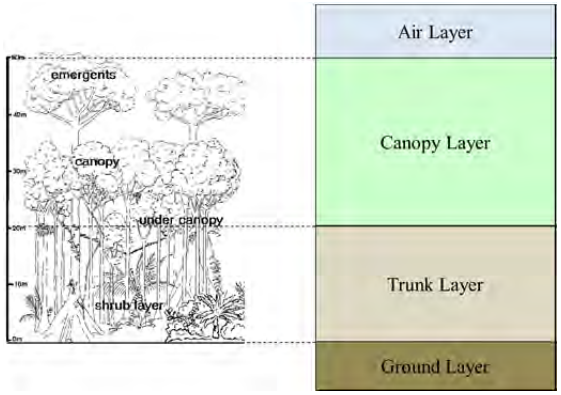

Figure 1. Layered model of forest (after [1], [2]).

Since the 1960s, there has been extensive research conducted to generate models for estimating propagation loss [3]. Several approaches have been used to investigate and model the propagation. The approaches include experimental, empirical, analytical, and computational electromagnetic methods (CEM). With the advancement in technology, computer processors were used to model the propagation loss. There are several possible configurations that occur when modeling the propagation loss, as depicted in Figure 2.

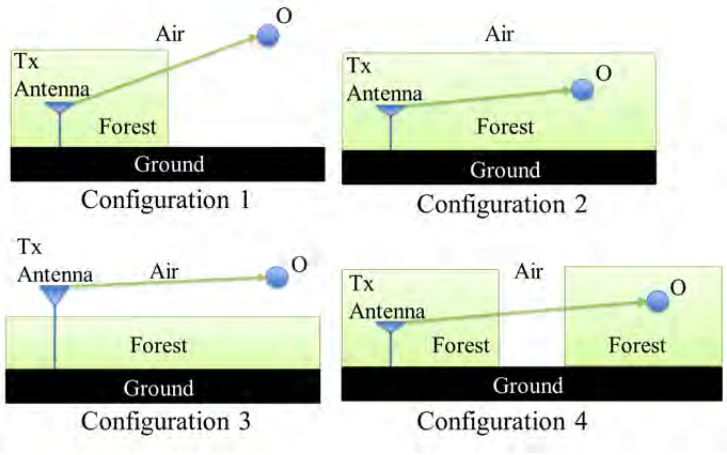

Figure 2. Possible configurations to model propagation loss (after [4]).

Each of the approaches exhibits individual merits that contribute to a solution addressing the problem. In the previous work by Chan [5], Computer Simulation Technology (CST) Microwave Studio (MWS) was used for path loss prediction in foliage. MWS is a three-dimensional modeling tool that solves the integral form of Maxwell's equations numerically. It was used to model the complex forest environment as a single layer dissipative slab as proposed by Tamir's work [6]. Simulated results suggest that CST software can be used to provide a rough approximation of the attenuation; however, the limitation of this technique is the high computational resources needed and time required for simulation of the large slab (i.e., one beyond several wavelengths).

In this thesis, an analytical method using the ray tracing method is used to model the propagation with the objective of overcoming the shortcomings of the previous work

[5]. The second objective is to determine the physical and electrical characteristics of the model that correspond to the scenario of interest.

With the assumption that the potential ionoshperic waves are negligible for a separation distance of less than 100 km, two electromagnetic (EM) wave propagation mechanisms were identified within the forest layer as depicted in Figure 3. The two wave components are the lateral wave component (path TABO) and the Geometrical Optics component (GO, direct and reflected waves). The formulation provided in [6] was used for lateral component computation. Additionally, modifications of the formulation used to compute the GO wave in [7] were made to minimize the overestimation of fields at near distances. The ray tracing model, a three-layered model as shown in Figure 3, was implemented in MATLAB. The three layers defined in the model are all homogeneous. Inputs of the geometry for the forest layer are performed by the user. The problem geometry setup is depicted in Figure 4. Besides the geometry inputs, the electrical properties of each layer are required from the user. It was found that only two reflections from the interfaces need to be considered.

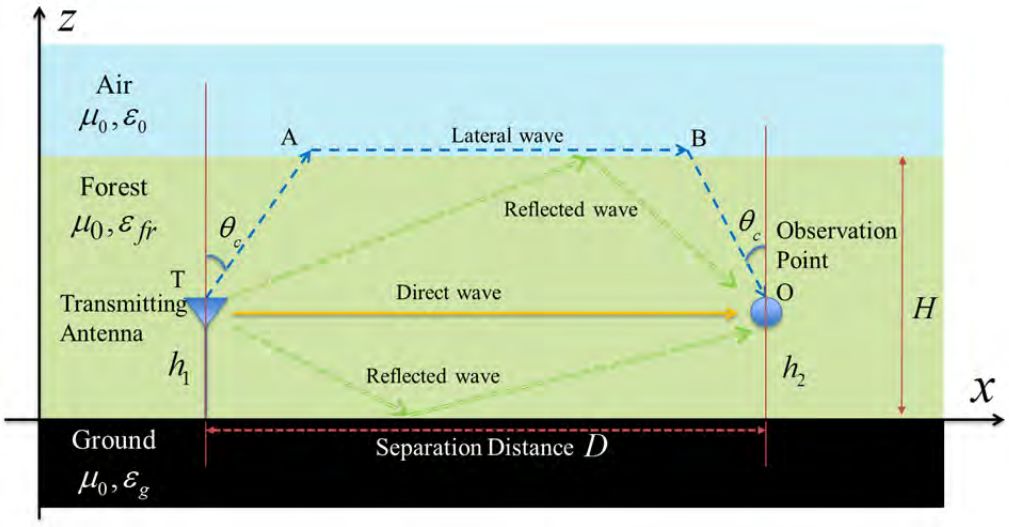

Figure 3. Propagation mechanism within foliage (after [6]).

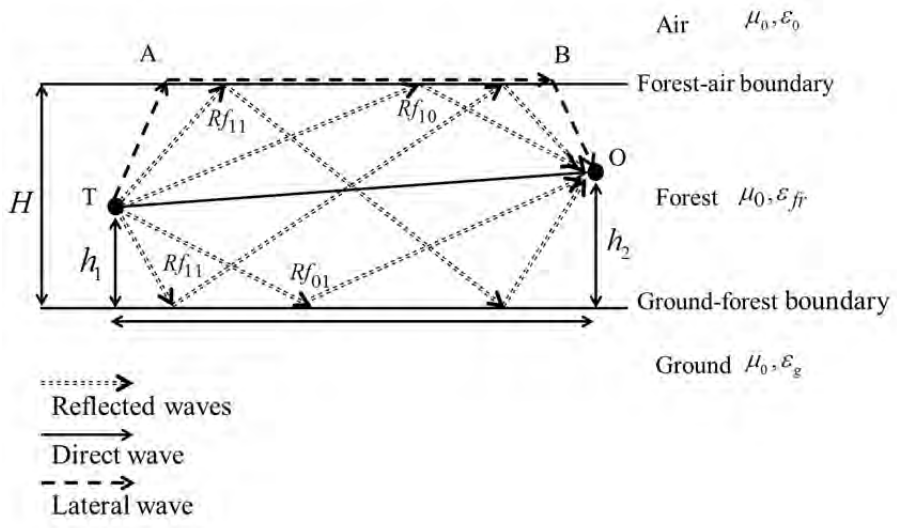

Figure 4. Ray tracing model.

Two cases were analyzed to validate the ray tracing model. The objective of Case I was to compute the average error between the measured data extracted from [7] based on the Sommerfeld solution and the results generated from the ray tracing model (see Table 1). The measured data were taken by fixing the height of the transmitting antenna to 3.96 m and varying the height of the receiver from 7.0 m to 28.96 m. The separation distance D was also kept constant at 1.6 km.

Table 1. Average error between measured data from [7] and ray tracing model with adjusted parameter.

	Average error compared between model and measured data			
	H-pol to H-pol		**V-pol to V-pol**	
Frequency (MHz)	**Sommerfeld solution**	**Ray tracing model**	**Sommerfeld solution**	**Ray tracing model**
25	0.60	0.82	0.30	0.90
50	0.80	0.23	0.40	0.48
100	0.90	0.97	0.40	0.72

The idea of using a homogenous medium to represent the forest layer provided satisfactory correlation to the measured data (within 1 dB) up to a frequency of 100 MHz.

The objective of Case II was to compute the root mean square (RMS) error between the measured data from two empirical models [8] (the Jansky and Bailey model,

and Tewari's model) and the ray tracing model. A RMS error value was introduced in [9] to provide a useful performance quantity. In Case II, both the heights of the transmitting antenna and observation points were fixed at 5.0 m. The separation distance was from 1.0 m to 4.2 km. Table 2 is populated with the resultant RMS error computed for each deterministic model for distances greater than 1.0 km.

Table 2. RMS Error for measured data at 50 MHz and D greater than 1.0 km.

Polarization	**Ray tracing model, δ_{RMS} (dB)**	**Tewari's empirical model, δ_{RMS} (dB)**	**JB model, δ_{RMS} (dB)**
V-pol	2.6869	2.4377	2.5979
H-pol	1.3415	1.3141	1.3813

In conclusion, the ray tracing model is able to provide good estimation of propagation loss up to 100 MHz in a forest environment. This model is applicable to propagation loss estimation for cases where the antennas are deployed more than 1.0 km apart. The advantage of this model over the previous model using CEM is its applicability to estimate the propagation loss at a distance beyond 1.0 km. Recommended future work includes exploring methods to determine effective parameters (permittivity and conductivity) of the forest layer and formulating models for the other configurations depicted in Figure 2. Lastly, to complement the empirical and analytical approaches, CEM models can be explored to address propagation losses within the 1.0 km range.

List of References

[1] L. W. Li, T. S. Yeo, P. S. Kooi, and M. S. Leong, "Radiowave propagation along mixed paths through a four-layered model of rain forest: an analytic approach," *IEEE Trans. on Antennas Propag.*, vol. 46, no. 7, pp. 1096–1111, 1998.

[2] L. o. t. Internet, "Learn on the Internet," [Online]. Accessed August 2, 2014. Available: http://www.geography.learnontheinternet.co.uk/images/ecosystems/crosssection1.gif

[3] Y. S. Meng, Y. H. Lee, and B. C. Ng, "Empirical near ground path loss modeling in a forest at VHF and UHF," *IEEE Trans. on Antennas Propag.*, vol. 57, no. 5, pp. 1461–1468, 2009.

[4] T. Tamir, “Radiowave propagation along mixed paths in forest environments,” *IEEE Trans. on Antennas Propag.*, vols. AP-25, no. 4, pp. 471–477, 1977.

[5] C. W. Chan, “Investigation of propagation in foliage using simulation techniques,” M.S. thesis, Department of Electrical and Computer Engineering, Naval Postgraduate School, Monterey, CA, September 2011.

[6] T. Tamir, “On radiowave propagation in forest environments,” *IEEE Trans. on Antennas Propag.*, vol. AP-15, no. 6, pp. 806–817, November 1967.

[7] Y. Li and H. Ling, “Numerical modeling and mechanism analysis of VHF wave propagation in forested environments using the equivalent slab model,” *Progress in Electromagn. Res.*, vol. 91, pp. 17–34, 2009.

[8] R. K. Tewari, S. Swarup, and N. R. Manujendra, “Radiowave propagation through rain forests of India,” *IEEE Trans. on Antennas Propag.*, vol. 38, no. 4, pp. 433–449, 1990.

[9] M. O. Al-Nuaimi and R. Stephens, “Measurements and prediction model optimization for signal attenuation in vegetation media at centimetre wave frequencies,” *Proc. in Microw., Antennas Propag.*, vol. 145, no. 3, pp. 201–206, 1998.

ACKNOWLEDGMENTS

Foremost, I would like to thank Professor David C. Jenn for his guidance and advice. His knowledge and guidance was the key to my completion of this thesis.

I would like to thank Professor Phillip E. Pace for agreeing to be the second reader of this thesis.

I would like to thank my wife, Irene Seah, for her relentless support and encouragement during my course of study. I would also like to thank my mother, Joo Khim, for her support and encouragement.

Lastly, I would like to thank Singapore Technologies (Electronics), and my superiors, Mr. Chay Wing Yew John and Mr. Ng Woon Wei, for providing this opportunity to pursue my master's degree at the Naval Postgraduate School.

THIS PAGE INTENTIONALLY LEFT BLANK

I. INTRODUCTION

A. RADIOWAVE PROPAGATION IN A FORESTED ENVIRONMENT

Radiowave propagation loss in wireless communication systems plays an important role in overall link performance. For applications where communicating terminals are immersed in a forested environment, the prediction of the propagation loss is very challenging. Tree trunks, leaves, and undergrowth in the forest are randomly distributed and can cause attenuation, scattering, diffraction, and absorption of the signal energy. This makes radiowave propagation through such environments a complex problem to model. Modeling of this propagation loss has been an area of interest since the 1960s [1].

There are various types of woodlands and each has characteristics that are different from one another due to climate differences. A classification of the different layers within a forested environment is depicted in Figure 1. These layers provide a simplified model for analyzing the problem [2]. If the variation within each level as a function of distance is small compared to the wavelength of the propagating wave, then an effective homogeneous medium can be defined for each layer.

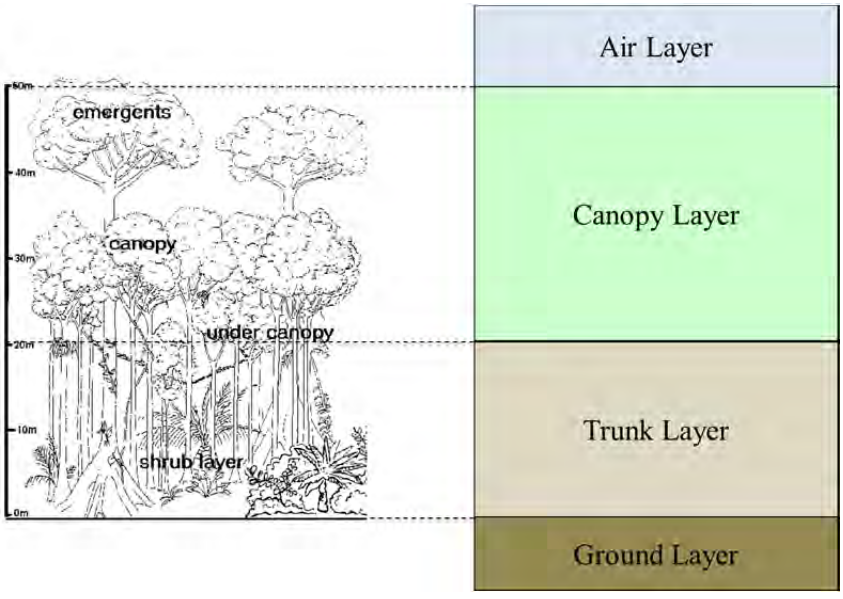

Figure 1. Layered model of the rain forest (after [2], [3]).

There are many important real-world applications that drive radiowave propagation studies in foliage. Examples are military operational scenarios that require communication systems to be deployed in forested environments, including unmanned ground sensors (UGS) and downlink communication from an unmanned aerial vehicle (UAV) to troops located within forest. Lastly, there is deployment of vehicular communication nodes within forested environments to relay information to dismounted soldiers [4].

In the context of non-military operations, there are search and rescue missions in forests [5] and also wireless sensor networks for agricultural applications [6]. These are just some examples of communication links that require consideration of the losses due to the scattering, diffraction, and attenuation within the forested environment.

B. BACKGROUND

Several approaches have been used to investigate and model the propagation loss characteristics of a complex forested environment. One of these approaches is experimental measurement. Numerous radiowave measurement studies have been conducted in the tropical rainforest located in Northern India, where the measured results were taken in the frequency range from 50 MHz to 800 MHz [7]. Other measurements were taken from central and southern parts of Thailand [8] at frequency ranges from 2 MHz to 400 MHz. The limitation to these measurements is that they cannot easily be extended to other types of forest.

Empirical models were also introduced for predicting the propagation loss from various sources. They include the International Telecommunication Union Recommendations (ITU-R) [9], Modified Exponential Decay (MED) model by Weissberger [10], and COST 235 model [11]. There are many other models in addition to these. The models are useful in providing a rough estimate of radiowave attenuation through vegetation.

Analytical methods have been used to determine the characteristics of radiowave propagation in a forested environment. Tamir [12] proposed that the complex forested environment can be modeled as a dissipative slab provided the wavelength at the

operating frequency is much smaller than the irregularities of the forested environment. This model, together with the theory on wave propagation in a stratified medium, led to the finding that the “tree top” wave propagation is the dominant mode compared to the direct and multipath waves within the forest. Leveraging this concept, there were subsequent works done using the same idea of treating the forested layers as homogenous, isotropic media [13], [14].

With the advancement in computer processors, the use of computational electromagnetic methods (CEM) has become an attractive tool to solve more complex real-world electromagnetic (EM) problems. Leveraging on this, the previous work by Chan [13] investigated simulation techniques for path loss prediction in foliage using Computer Simulation Technology (CST) Microwave Studio (MWS). MWS is a three-dimensional modeling tool that solves the integral form of Maxwell’s equations numerically. It was used to model the complex forest environment as a single layer dissipative slab as proposed by Tamir’s work. Simulated results suggest that the model of the slab using the CST software can be used to provide a rough approximation of the attenuation. The limitation of this technique is the high computational resources needed and time required for simulation of large slab (i.e., one beyond several wavelengths).

Other approaches have been used to model the radiowave characteristics in a forested environment. The frequency range of the early works is the very high frequency (VHF) band (30 to 300 MHz) where the wavelength is relatively long (1.0 m to 10.0 m). With the congestion of spectrum usage in the VHF band and the introduction of digital communication systems into the communication community, there has been a shift of frequency usage to the ultra-high frequency (UHF) band [15]. Operating at higher frequencies in the forest environment poses different challenges, as the wavelengths are shorter for higher frequencies. The work done by Li [14] is of particular interest. The use of ray tracing methods suggests that the numerical results for the transmission loss and the time delay versus range exhibit good agreement with the numerical Sommerfeld integral solutions. Further modeling of the propagation using the ray tracing method is presented in this thesis.

C. THESIS OBJECTIVE

In the previous study by Chan [13], MWS was used to model a homogeneous lossy dielectric slab as a representation of the forest medium. Two important parameters (conductivity and permittivity) used in modeling the slab that determine the forest electrical characteristics are discussed in this thesis. A rough approximation for radiowave propagation at short distances within the forest medium was achieved. One of the limitations in using CEM to model the radiowave propagation loss is the long processing time and large amount of computer memory required. One objective of this thesis is to explore an alternative approach that removes this limitation.

A deterministic model based on ray tracing methods is investigated in this research. This model is used to generate the lateral waves as well as the geometric optic (GO) waves which are summed at the observation point, as illustrated in Figure 2.

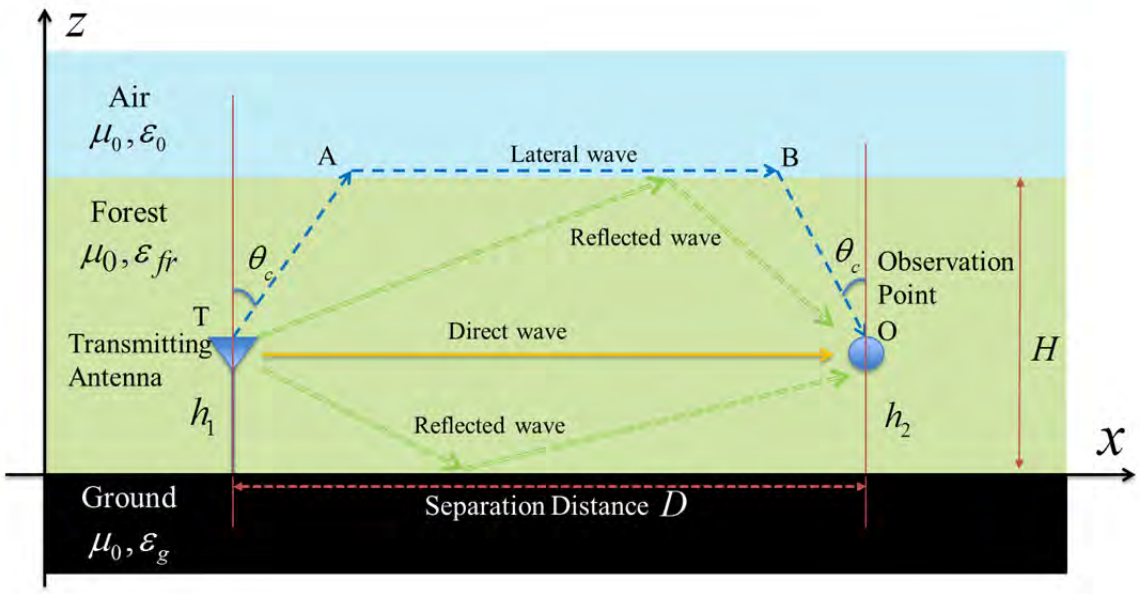

Figure 2. Illustration of propagation mechanisms (after [12]).

Simulation results from the code generated in MATLAB software are used to compare with measured data extracted from [7] and [14]. This is to re-establish the finding in [12] that a homogeneous slab is applicable to compute propagation loss up to 100 MHz within the VHF band.

D. THESIS OUTLINE

There are five chapters in this thesis and they are organized in the following sequence.

In Chapter I, the background and objectives of the thesis was presented.

In Chapter II, the EM wave propagation mechanisms within the forest layer, as well as the formulations for the different mechanisms used to describe the wave propagation, are discussed.

In Chapter III, we document the list of assumptions and considerations for the ray tracing model. Formulation of the model are described in detail.

In Chapter IV, comparisons of the simulated results are made with measured data and some observations are offered based on the results.

Finally, in Chapter V, a summary and conclusions with recommendations for future work are presented.

THIS PAGE INTENTIONALLY LEFT BLANK

II. METHODOLOGY USED FOR MODELING

In this chapter, the various analytical methods employed to study the propagation loss for communication links within the forest in the VHF and UHF bands are summarized. A set of possible configurations for communication systems operating within or outside a forest environment is defined. A summary of EM plane wave theory is provided to illustrate the effect of various parameters.

Besides reviewing the analytical methods, the propagation mechanisms that are present within the forest environment are described. A list of empirical models used in the study of propagation loss from foliage are presented, to be used as part of the tools to validate our model

A. ANALYTICAL METHODS

Analytical approaches have been used in modeling propagation loss. Deterministic models use different solution techniques to compute the propagation loss for the various configurations depicted in Figure 3 [16]–[19].

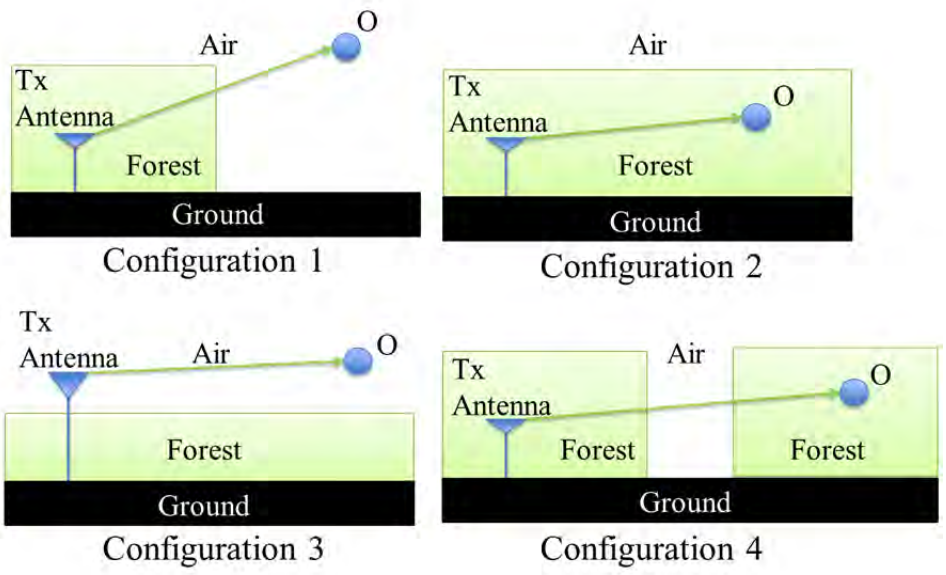

Figure 3. Various configurations for deterministic modeling (after [18]).

Most of the analytical modeling uses an infinitesimal dipole as the transmitting antenna or for both transmitting and receiving. The point O labeled in Figure 3 is either the location of a receiving antenna or simply a point in space for computation of electric field strength. The calculation of received power requires that an antenna be specified; however, the calculation of field strength does not.

The initial work by Tamir suggested that the upper limit of the operating frequency for the foliage block model is 100 MHz [12]. In his later work with Dence [20], this upper limit was extended to 200 MHz. This extension of upper frequency limit was obtained by including the ground's effect into the initial closed form lateral wave equation derived in [12]. A different method was reported by Palud [21] in 2004, and he compared his method used with the results reported in [18]. Palud used the full-wave Parabolic Equation (PE) algorithm in treating the forest as a lossy medium characterized by its permittivity and conductivity. The model was able to predict the propagation loss in either Configuration 1 or Configuration 2 depicted in Figure 3. The results for Configuration 1 showed noticeable asymmetry in the uplink and downlink and did not match to the results that were reported in [18]; however, results based on Configuration 2 showed good agreement. Liao and Sarabandi [16] investigated the problem by using a surface field integration technique. Configuration 1 was studied, and it was found that at low observation heights, the solution underestimates the received field at the observation point compared to [18] due to the assumption made by Tamir that all energy arriving at the canopy edge is assumed to be coupled entirely towards the observation point for both polarizations.

Given the same idea of a homogeneous medium to represent the forest layer, there are various deterministic models proposed for planar stratified media. A three-layered model using Green's dyadic function to predict propagation loss was reported in [22]. The theoretical results were in good agreement with the available experimental data at 6 MHz. Within the same time frame, Cavalante used the same method and modeled the propagation loss using four homogenous layers [23]. This four-layer model takes into account the vertical non-homogeneities of the forests in order to extend the prediction accuracy as high as 250 MHz. Subsequently, Seker and Scheider [15] used the Hertz

potential method applied to anisotropic stratified media to predict the propagation loss in a forest environment. The range of frequencies was from 20 MHz to 2,000 MHz due to the high level of interest in several wideband digital radio systems [24]. However, results from both [15] and [24] were not compared to any measured data at the time.

Extensive analytical study on the propagation loss at both VHF and UHF were conducted by Li [1]. This extensive study of radiowave propagation in a four-layered model uses Green's dyadic function to solve the problem. Li concluded that the lateral waves at the forest-air boundary are the dominant waves compared to the other lateral waves propagating along the air-canopy, trunk-canopy and ground-trunk boundaries. The high attenuation of lateral waves along the ground-trunk boundary is due to the high conductivity of the ground layer [19].

A summary of the various solution approaches and the applicable configurations defined in Figure 3 are tabulated in Table 1.

Table 1. Summary table for the various analytic methods used to model propagation loss.

Method	Configuration with reference to Figure 3	Number of Layers	Planar Stratified Mediums
Parabolic Equation Algorithm [21]	1, 2	2	Homogeneous
Ray Tracing [18]	2	2	Homogeneous
Sommerfeld Integral Solution [14]	2	3	Anisotropic
Dyadic Green's Function [19] , [22] [23] and [25]	2	3, 4	Homogeneous
Surface Field Integral Technique [16]	1	2	Homogeneous
Hertz Potential Method [15] and [24]	2	4	Anisotropic

We use a ray tracing method to model a three-layer planar stratified medium as shown in Figure 2, and the details of the model are covered in Chapter III. For our analytical approach, we require measured or estimated electrical data as inputs for properties of the forest medium. A review of the various approaches used to obtain the electrical properties of the forest medium was performed and the values reported in [26]. This is discussed in Section C of this chapter.

B. EM PLANE WAVE PROPAGATION

EM waves consist of two coupled, time-varying vector fields, $\vec{E}$ (electric) and $\vec{H}$ (magnetic). The time dependence $e^{j\omega t}$ is assumed in our analysis and suppressed throughout this thesis. These fields are governed by physical laws described by Maxwell's equations. As an illustration of the fields in space, let the direction of propagation of the wave be in the positive $\hat{z}$-direction. The $\vec{E}$ fields and $\vec{H}$ fields are pointing in the positive $\hat{x}$- and positive $\hat{y}$-directions, respectively, as shown in Figure 4.

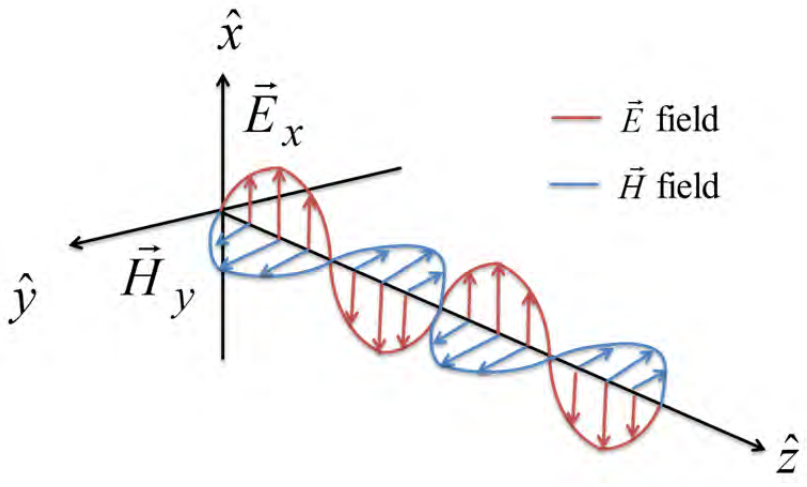

Figure 4. EM wave propagating in positive $\hat{z}$-direction.

Plane waves are assumed in our discussion of wave propagation. The wave fronts are infinite parallel planes of constant amplitude normal to the phase velocity vector. Plane wave approximations are adequate when the extent of the boundaries between the

layers are large compared to wavelength. Then the reflection and refraction of a spherical wave can be considered locally planar.

In lossless media, Maxwell's equations in phasor form relate the $\vec{E}$ and $\vec{H}$ fields as [27]:

$$\nabla \times \vec{E} = -j\omega\mu\vec{H} \tag{1}$$

$$\nabla \times \vec{H} = -j\omega\varepsilon\vec{E} \tag{2}$$

where $\omega = 2\pi f$ is the angular frequency in rad/s, μ is the permeability of medium, ε is the permittivity of the medium, and $j = \sqrt{-1}$.

The wave equations are derived from Eq. (1) and Eq. (2), resulting in the final form expressed as [27]:

$$\nabla^2\vec{E} + \omega^2\mu\varepsilon\vec{E} = 0 \tag{3}$$

$$\nabla^2\vec{H} + \omega^2\mu\varepsilon\vec{H} = 0\ . \tag{4}$$

Now the wavenumber k of the medium is expressed as:

$$k = \omega\sqrt{\mu\varepsilon} \tag{5}$$

where values of μ and ε are real in a lossless medium.

For plane waves in a lossy medium, Maxwell's equations can be written as [27]:

$$\nabla \times \vec{E} = -j\omega\mu\vec{H} \tag{6}$$

$$\nabla \times \vec{H} = j\omega\varepsilon\vec{E} + \sigma\vec{E} \tag{7}$$

where σ is the conductivity of the medium, $\varepsilon = \varepsilon_r\varepsilon_0$ where ε is the permittivity and ε_r is the relative permittivity. The complex permittivity is defined as [12]:

$$\varepsilon_c = \varepsilon_0\varepsilon_{r_c} = \varepsilon_0\left(\varepsilon_r - j\frac{\sigma}{\omega\varepsilon_0}\right) \tag{8}$$

where ε_{r_c} is the complex relative permittivity of the lossy medium. The resulting wave equation for $\vec{E}$ is now expressed as:

$$\nabla^2\vec{E} + \omega^2\mu\varepsilon\left[1 - j\frac{\sigma}{\omega\varepsilon}\right]\vec{E} = 0\ . \tag{9}$$

The difference between Eq. (3) and Eq. (9) is that the complex permittivity ε_c introduced by the lossy medium makes the wavenumber a complex number. This complex number is defined as the propagation constant γ expressed as:

$$\gamma = \alpha + j\beta = j\omega\sqrt{\mu\varepsilon}\sqrt{1 - j\frac{\sigma}{\omega\varepsilon}} \tag{10}$$

where α is the attenuation constant and β is the phase constant.

With the assumption that the wave is propagating in the positive $\hat{z}$-direction, Eq. (9) can be reduced to:

$$\frac{\partial^2 E_x}{\partial z^2} - \gamma^2 E_x = 0 \tag{11}$$

and the solution for $E_x(z)$ is:

$$E_x(z) = E^+ e^{-\gamma z} + E^- e^{\gamma z}. \tag{12}$$

The exponential factor for travelling waves in the positive $\hat{z}$-direction is expressed as:

$$e^{-\gamma} = e^{-\alpha z} e^{-j\beta z}. \tag{13}$$

The ratio between the $\vec{E}$ and $\vec{H}$ fields determines the intrinsic impedance. Computed value for impedance in free space is $\eta_0 = \sqrt{\mu_0 / \varepsilon_0} = (120\pi)\ \Omega$. The impedance of the forest is expressed as [27]:

$$\eta_f = \eta_0 \Big/ \sqrt{\varepsilon_{fr_c}} \approx \frac{120\pi}{\sqrt{\varepsilon_{fr_c}}} \tag{14}$$

where $\varepsilon_{f_{r_c}}$ is relative complex permittivity of the forest layer expressed as [12]

$$\varepsilon_{f_{r_c}} \approx \varepsilon_{f_r} - j60\sigma_f\lambda \tag{15}$$

where ε_{f_r} is the relative permittivity of the forest layer, σ_f is the conductivity of the forest layer and λ is the wavelength in meters.

Until this point, we have covered the theory required to compute $\vec{E}$ within a medium with a given dielectric constant and conductivity. To address the waves reflected off the boundaries of the medium, there is another parameter to be considered. The computation of the reflection coefficient for waves reflected off of a plane interface

between two dielectric regions is depicted in Figure 5. Based on the well-known Snell's laws of reflection and refraction [27]:

$$\theta_i = \theta_r \tag{16}$$

$$\eta_1 \sin\theta_i = \eta_2 \sin\theta_t \tag{17}$$

where θ_i is the incident wave angle from the normal to the plane interface, θ_r is the reflected wave angle, θ_t is the transmitted wave angle or refracted angle. Lastly, η_1 and η_2 are the impedances for medium 1 and medium 2, respectively.

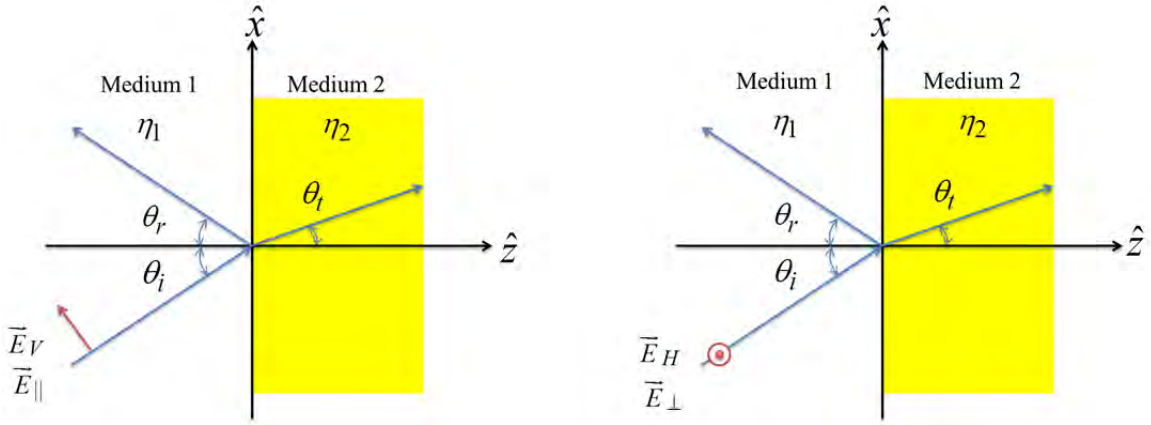

Figure 5. Polarization for electric field vector (after [27]).

The polarization for the EM wave is with reference to the plane of incidence ($\hat{x}-\hat{z}$ plane) as shown in Figure 5. For vertical polarization (V-pol), the vector $\vec{E}_V$ is parallel to the $\hat{x}-\hat{z}$ plane. The component of $\vec{E}_H$ perpendicular to the $\hat{x}-\hat{z}$ plane is defined as horizontal polarization (H-pol). These terms originate from low grazing angles $\left(\theta_i \to 90°\right)$. The parallel component becomes vertical with respect to the interface. The perpendicular component is horizontal.

The reflection coefficient for vertical polarization is expressed as [27]:

$$\Gamma_{||} = \Gamma_V = \frac{\eta_2 \cos\theta_t - \eta_1 \cos\theta_i}{\eta_1 \cos\theta_t + \eta_2 \cos\theta_i} \tag{18}$$

and the reflection coefficient for horizontal polarization is expressed as [27]:

$$\Gamma_{\perp} = \Gamma_H = \frac{\eta_2 \cos\theta_i - \eta_1 \cos\theta_t}{\eta_2 \cos\theta_i + \eta_1 \cos\theta_t} \tag{19}$$

where η_1 and η_2 are the wave impedances for medium 1 and medium 2, respectively, and θ_t is related to θ_i by Eq. (17).

C. ELECTRICAL PROPERTIES OF THE MEDIA

A summary of the various approaches used in determining the electrical properties of the forest is described in [26]. Open-wire transmission lines (OWLs) were used as probes to make actual site measurements of the electrical properties of a forest by Parker and Hagn [28] in 1966. The study using the OWL method was restricted to 75 MHz. Both Parker and Hagn also conducted a feasibility study on using the parallel plate capacitor technique and cavity technique to estimate the electrical properties of the forest in the same study published in 1966. The parallel plate capacitor technique was found to have many limitations, and the cavity technique was not suitable [26]. Another approach introduced to determine these electrical properties is the inverse method. This method utilizes the data collected from measurements such as antenna patterns within vegetation, transmission loss over distance, wave impedance, or attenuation variations to estimate the values of relative permittivity ε_{f_r} and conductivity σ_f of the forest slab. The electrical properties of the forest medium obtained via the inverse method from [26] are tabulated in Table 2. Electrical properties from each site are different, as expected, as well as frequency dependent.

Table 2. Electrical properties of forest medium (after [26]).

Measurement Site	**Source**	**Frequency (MHz)**	**Relative permittivity ε_{f_r}**	**Conductivity σ_f (mS/m)**	**Attenuation constant α_f (Np/m)**
India (Northern India)	Tewari (1982)	50	1.065	0.135	0.0246
		200	1.055	0.145	0.0266
		500	1.040	0.160	0.0296
		800	1.040	0.160	0.0296
Pak Chong (Northern Thailand)	Jansky and Bailey (1966-73)	2	1.010	0.045	0.0083
		400	1.010	0.045	0.0084
Satun (Southern Thailand)	Jansky and Bailey (1966-73)	2	1.010	0.035	0.0065
		400	1.010	0.035	0.0066

D. ELECTROMAGNETIC WAVE PROPAGATION MECHANISM FOR FOREST LAYER

The two main propagation mechanisms used to characterize the communication link within the forest layer are lateral waves and Geometrical Optics (GO) waves as described in [14]. Lateral waves are found propagating along the air-forest boundary (path AB) depicted in Figure 2. This lateral wave is generated by the refraction of the GO wave incident at a critical angle θ_c and propagates along the path AB. As it propagates along the forest-air boundary, it radiates back into the forest layer at the same critical angle.

This critical angle is dependent on the relative permittivity of the forest ε_{f_r} defined as [12]:

$$\theta_c = \sin^{-1}\left(\frac{1}{\varepsilon_{f_r}}\right). \tag{20}$$

The real part of the complex permittivity of the forest layer is used in Eq. (20). To obtain the lateral wave component travelling along the forest-air boundary, the GO wave traveling towards the forest-air boundary at this critical angle assumes the imaginary term

of the complex permittivity is very much smaller compared to the magnitude of the complex permittivity [29].

Multiple reflected GO waves are generated within the forest layer either via reflections off the forest-air boundary or the ground-forest boundary. The effect of the reflected GO waves with more than two reflections off the same boundaries has little effect on the overall electric field. There are two main contributing factors to this claim. The first is the high attenuation. Let us take the India forest example from Table 2. For 50 MHz a direct line - of - sight communication link with a distance of 100 meters apart, the attenuation constant is about 0.0246 Np/m. At this distance (100 m), the total loss is computed by multiplying the attenuation constant value with a conversion factor of 8.686. This results in the total attenuation of 21 dB.

The second contributing factor is the reflection coefficient. There is multiplication of the reflection coefficient factor in addition to the attenuation. Each reflection coefficient multiplication reduces the field. The field is further attenuated by the additional path traveled in the lossy foliage to the next reflection point; thus, we are only taking into account waves that have reflections off the boundaries at most once.

E. EMPIRICAL MODELS

In this section, seven models are discussed: the Weissberger model, International Telecommunication Union – Recommended (ITU-R) model, fitted ITU-R model, COST 235 model, lateral ITU-R model, Jansky and Bailey model, and Tewari's empirical model. The total propagation loss through the vegetation for some of the models (Weissberger, ITU-R, Fitted ITU-R, COST235, and Lateral ITU-R) requires the addition of the plane earth attenuation *PE* defined as:

$$PE(\text{dB}) = 40\log_{10}(D) - 20\log_{10}(h_1) - 20\log_{10}(h_2) \tag{21}$$

where h_1 is the height of transmitting antenna in meters and h_2 is the height of observation point in meters. The separation distance D is assumed to be very large compared to $h_1 + h_2$ [30].

(1) Weissberger Model

The Weissberger model was introduced in 1982 to provide a better prediction from the exponential decay (EXD) model [10]. In the report, it was called the modified exponential decay (MED) model and is applicable for an operational scenario where both transmitting and receiving antennas are immersed in temperate-latitude forests filled with dense, dry, in-leaf trees. The model predicts the foliage loss excluding the plane earth losses. The frequency can be from 230 MHz to 95 GHz. Therefore, addition of the plane earth model losses is required.

The empirical model is expressed as:

$$L_W(dB) = \begin{cases} 1.33 f_{GHz}^{0.284} D^{0.588}, & 14 \text{ m} \le D \le 400 \text{ m} \\ 0.45 f_{GHz}^{0.284} D, & 0 \text{ m} \le D < 14 \text{ m} \end{cases} \quad (22)$$

where L_W is the vegetation loss in dB, f_{GHz} is the frequency in GHz and D is the separation distance in meters between the transmitting antenna and observation point.

(2) International Telecommunication Union – Recommendation (ITU-R) Model

The ITU-R model [9] was developed from measured data in the UHF band in 1986. In measurement setup, the transmitting antenna, and observation point are separated by a small grove of trees with depth less than 400 m. The frequency can be from 200 MHz to 95 GHz. The majority of the signal propagates through the grove of trees, and the empirical model is expressed as:

$$L_{ITU-R}(dB) = 0.2 f^{0.3} D^{0.6} \quad (23)$$

where L_{ITU-R} is the vegetation loss in dB and the frequency f is in MHz.

(3) Fitted ITU-R Model

This model was proposed by Al-Nuaimi and Stephens [31] from optimization of the ITU-R model by measurements made at 11.2 GHz and 20 GHz at two foliation states (in-leaf and out of leaf). The expression for the empirical model is:

$$L_{FITU-R} = \begin{cases} 0.37 f^{0.18} D^{0.59}, & \text{out of leaf} \\ 0.39 f^{0.39} D^{0.25}, & \text{in leaf} \end{cases} \quad (24)$$

where L_{FITU-R} is the vegetation loss in dB and the frequency f is in MHz.

(4) COST 235 Model

The COST 235 model [11] is proposed based on measured data between 9.6 GHz and 57.6 GHz through a small grove of trees less than 200 m. The empirical model is expressed as:

$$L_{COST}(dB) = \begin{cases} 26.6 f^{-0.2} D^{0.5}, & \text{out of leaf} \\ 15.6 f^{-0.009} D^{0.26}, & \text{in leaf} \end{cases} \quad (25)$$

where L_{COST} is the vegetation loss in dB and the frequency f is in MHz.

(5) Lateral ITU-R Model

The lateral ITU-R (LITU-R) model was proposed by Meng [32] to analyze the effect of foliage and the ground's effect on the propagation loss over a tropical plantation at both VHF and UHF bands. The modified ITU-R model is express as:

$$L_{LITU-R}(dB) \cong 0.48 f^{0.43} D^{0.13} \quad (26)$$

where L_{LITU-R} is the vegetation loss in dB and the frequency f is in MHz.

(6) Jansky and Bailey Model

The Jansky and Bailey (JB) model was developed based on the measurement data from a tropical forest in Pak Chong, Thailand [10]. The model applies to Configuration 2 in Figure 3 where both the transmitting antenna and observation point are immersed within the forest layer. The frequency can be from 25 MHz to 400 MHz. It can be adapted to either polarization with the heights for both transmitting and receiving antennas between 2.0 and 7.0 m. The range of the separation distance D is defined from 8.0 m to 1.6 km.

The loss expression for the JB model is [10]:

$$L_{JB}(dB) = 36.57 + 20\log_{10} f - 20\log_{10}\left[\frac{A_{JB}e^{-1609a_{JB}D_{mile}}}{D_{mile}} + \frac{B_{JB}}{D_{mile}^2}\right] \qquad (27)$$

where D_{mile} is the separation distance between the transmitting and receiving antennas in miles and L_{JB} is the total transmission loss in dB and the frequency f is in MHz. A_{JB} and B_{JB} are constants obtained empirically from the measured data. These constants are listed in Table 3.

Table 3. Constants for the JB Model (after [10]).

Frequency (MHz)	**Polarization**	a_{JB} **(dB/m)**	A_{JB}	B_{JB}
25	V-pol	0.0	0.0	0.002120
50	V-pol	0.0	0.0	0.001060
100	V-pol	0.045	0.615	0.000529
250	V-pol	0.050	0.759	0.000443
400	V-pol	0.055	1.020	0.000523
25	H-pol	0.0	0.0	0.004240
50	H-pol	0.0	0.0	0.004240
100	H-pol	0.020	0.472	0.005510
250	H-pol	0.025	0.774	0.000588
400	H-pol	0.035	1.110	0.000598

(7) Tewari's Empirical Model

Tewari's empirical model was developed using the measured data made in a reserve forest near Dehradun, Northern India [7]. The model addresses the exponential decay characteristics for forest depths less than 400 m. It was suggested that beyond the nominal 400 m, received signals from the transmitting antenna were partially via the lateral mode. Similar to that of the JB model, there is also a table of constants, shown in Table 4, applied for V-pol and H-pol. The applicable range of this model is from 40 m to 4 km. The frequency range is from 50 MHz to 800 MHz.

Table 4. Constants for the Tewari's empirical model (after [7]).

Frequency (MHz)	**Polarization**	a_T **(dB/m)**	A_T	B_T
50	V-pol	0.0	0.0	1.9170
200	V-pol	0.0125	0.4989	1.8358
500	V-pol	0.0135	0.3658	0.9040
800	V-pol	0.0140	0.2661	0.5331
50	H-pol	0.0	0.0	7.3670
200	H-pol	0.0110	0.8201	5.0450
500	H-pol	0.0138	0.6571	1.4304
800	H-pol	0.0152	0.4491	0.6291

The loss expression for Tewari's empirical model is [7]:

$$L_T(dB) = -27.57 + 20\log_{10} f - 20\log_{10}\left[\frac{A_T e^{-a_T D}}{D} + \frac{B_T}{D^2}\right] \tag{28}$$

where L_T is the total transmission loss in dB and the frequency f is in MHz.

In summary, we have described various configurations for deterministic modeling of propagation loss due to the presence of vegetation. A summary of the various approaches with reference to [1] was presented. The various analytical models presented were focused on the study of lateral waves and the waves generated in the VHF and UHF bands. Multiple planar media were utilized to characterize the different layers of the forest like the trunk and canopy layers. As the frequency of interest is increased to millimeter waves, the lateral wave over large forests can no longer exist. This leads to the use of CEM to provide solutions to the intractable mathematical formulations but also demands more computational resources.

The ray tracing method used to predict the propagation loss within a forest was introduced. We shall make use of this knowledge to formulate the model in Chapter III. Different approaches were used to determine the electrical properties of the forest layer. These electrical properties are site specific, and electrical properties for two sites were given in Table 2. This table is consulted again in our analysis in Chapter IV. Finally, we have presented the empirical models used to predict the propagation loss though the

foliage. We make use of the measured data to compare with our ray tracing model in Chapter IV.

THIS PAGE INTENTIONALLY LEFT BLANK

III. RAY TRACING MODEL

In this chapter, we list the assumptions and considerations of the ray tracing model and discuss the formulation of the model. Next, we elaborate on the modification the model suggested in [14] for computing the total electric field for the GO wave component. A set of general equations used to compute the path length for each GO wave with up to *N* reflections within the forest layer is described. A lateral wave component introduced by [12] is described and examined for its applicability to both polarizations.

A three-layer deterministic model is generated using MATLAB to compute the radiowave propagation loss. This model is setup for Configuration 2 from Figure 3, where both the transmitting antenna at T and observation point located at O are immersed within the forest layer as shown in Figure 6.

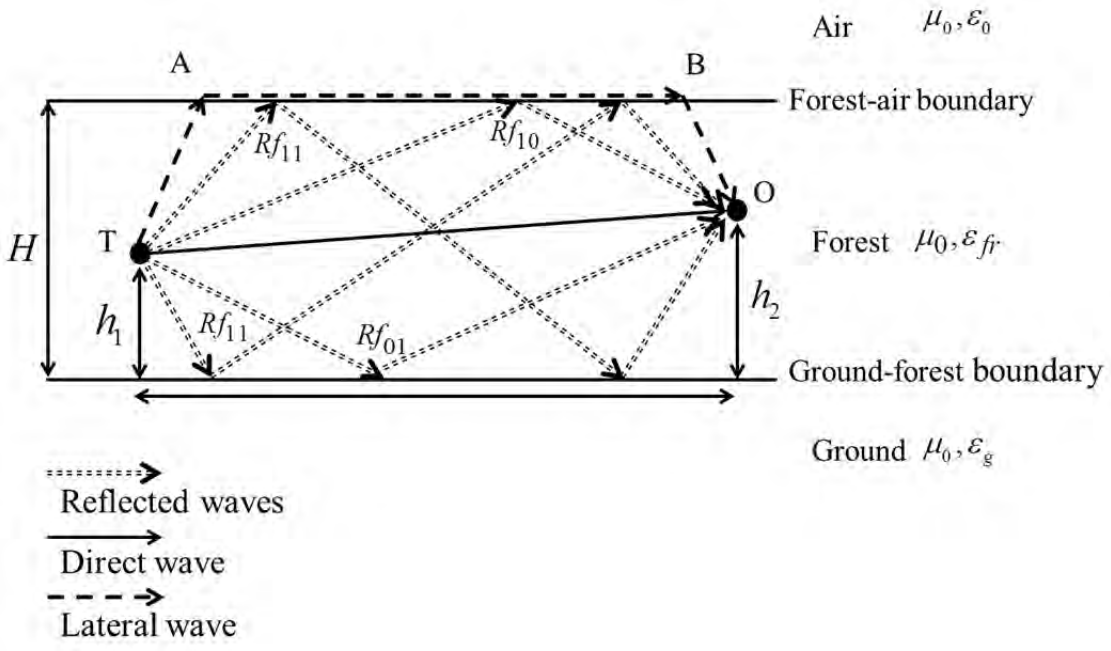

Figure 6. Ray tracing model.

A. ASSUMPTIONS AND CONSIDERATIONS

For the computation of the multi-bounce waves within the forest layer, reflections from the edges of forest layer are negligible and, thus, not taken into consideration [18]. This assumption is valid when the transmitting antenna and observation point are far away from the edge of the forested environment.

Only the primary lateral wave contribution and the single and double bounce rays are taken into consideration for this model. As discussed previously, the longer reflected path distance that occurs with each bounce within the forest attenuates the longer reflected paths more than the shorter reflected paths. Moreover, with the multiplication of additional reflection coefficient factors, we can assume that higher orders of the reflected waves (more than one bounce off the same boundary) can be ignored.

In order to model the forest as a uniform, continuous medium, the wavelength must be sufficiently large compared to the forest depth. Wavelength is dependent on the frequency of operation, and the maximum usable frequency of interest for our model is 100 MHz, which is the same criterion as Tamir [12].

The complex permittivity of the forest layer determines the refraction angle at the boundary layers between the forest and air. The real part of the complex permittivity is used to determine this angle.

There is potentially an ionospheric wave contribution, but it is not taken into consideration in the computation as it is negligible compared to the lateral waves. This assumption is valid when the distance between the transmitter and observation point is less than 100 km [20].

B. MODEL FORMULATIONS

The ray tracing model gives the total field strength of wave components emitted from the transmitting antenna at the observation point. The computed values of field strength produced by the propagation mechanisms described in Chapter II are summed at the observation point. The first component computes the field strengths from both direct and the multipath rays bounced within the forest layer, and the second component

computes the total field strength generated by the lateral waves formed via the ground bounce induced and primary lateral wave from the source.

A set of equations was generated to compute the path length between the transmitter and observation point. We explain the modification of the EM wave equation from [14] for the GO component in this section.

1. Propagation Constant

From the electromagnetic theory [27], the complex propagation constant of EM waves for a lossy medium consists of real and imaginary parts, where the real part is the attenuation constant and the imaginary part is the phase constant. Substituting the complex permittivity of the forest medium ε_{f_c} into Eq. (10), we find that the real part of the complex propagation constant, that is, the attenuation constant in (Np/m) of the forest layer, can be expressed as [26]:

$$\alpha_f = \left(\frac{1}{2} \left(\frac{\omega}{1/\sqrt{\mu_0 \varepsilon_0}} \right)^2 \left\{ \left[{\varepsilon_{f_r}}^2 + \left(\frac{\sigma_f}{\omega \varepsilon_0} \right)^2 \right]^{1/2} \right\} - \varepsilon_{fr} \right)^{1/2} \tag{29}$$

where μ_0 and ε_0 are the permeability and permittivity for free space, respectively. The imaginary part is the phase constant β_f (rad/s) of the forest layer is expressed as [26]:

$$\beta_f = \left(\frac{1}{2} \left(\frac{\omega}{1/\sqrt{\mu_0 \varepsilon_0}} \right)^2 \left\{ \left[{\varepsilon_{fr}}^2 + \left(\frac{\sigma_f}{\omega \varepsilon_0} \right)^2 \right]^{1/2} \right\} + \varepsilon_{fr} \right)^{1/2} . \tag{30}$$

2. Path Length Computation

There are an infinite number of waves that bounce off the forest-air and the forest ground boundary. There are many applications that can use the ray tracing method to determine effects in the communication link such as fading and multipath. Our application to model the reflected waves within the forest layer is less complex than many other multipath problems because we have only two parallel interfaces to consider. A set of general equations is derived in the process of determining the path length

between the transmitter and observation point. Let m be the number of bounces off the forest-air boundary and n be the number of bounces off the ground-forest boundary. An example of four possible cases in computing the path length is shown in Figure 7. The allowed ray trajectories are obtained by forcing Snell's law to be satisfied at each reflection point.

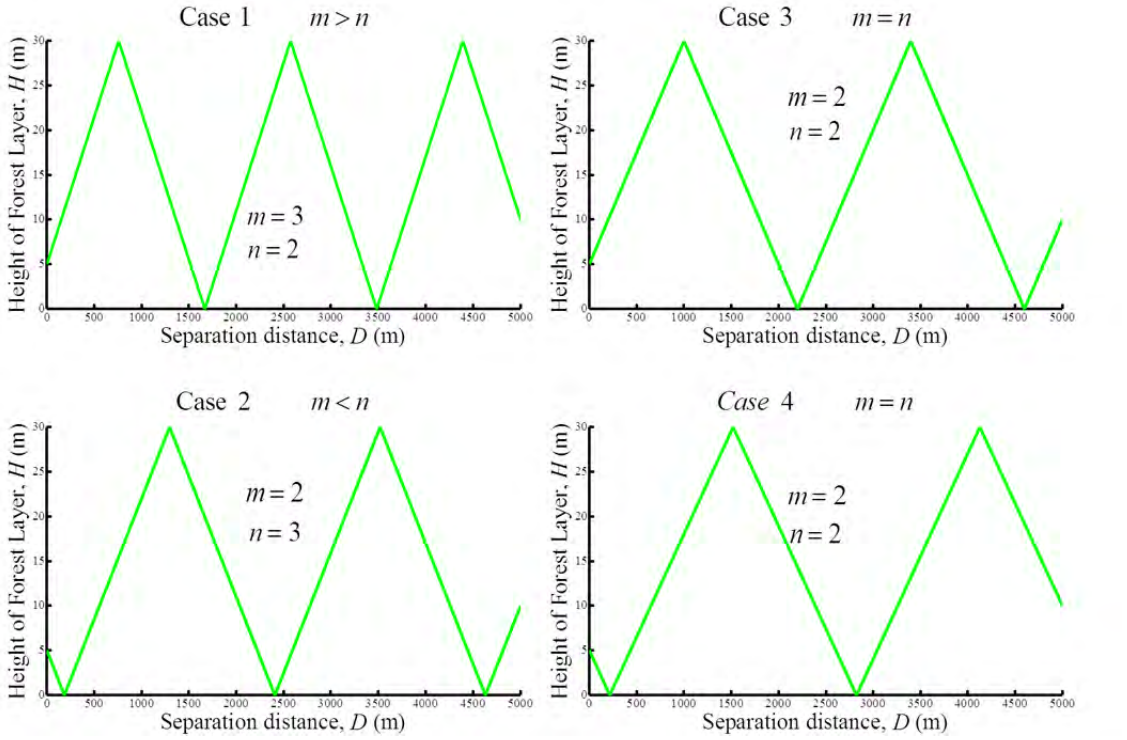

Figure 7. Four possible cases for the path length computation.

For case 1 where $m > n$:

$$D = x_1 + x_2\left(m + n - 1\right) + x_3 \tag{31}$$

$$\frac{H - h_1}{x_1} = \frac{H}{x_2} = \frac{H - h_2}{x_3} \tag{32}$$

$$x_3 = \frac{D}{\dfrac{H - h1}{H - h_2} + \left(m + n - 1\right)\dfrac{H}{H - h_2} + 1} \tag{33}$$

$$Rf_{mn} = \left(m + n - 1\right)\sqrt{H^2 + {x_2}^2} + \sqrt{\left(H - h_1\right)^2 + {x_1}^2} + \sqrt{\left(H - h_2\right)^2 + {x_3}^2}\ . \tag{34}$$

For case 2 where $m < n$:

$$D = x_1 + x_2\left(m+n-1\right) + x_3 \tag{35}$$

$$\frac{h_1}{x_1} = \frac{H}{x_2} = \frac{h_2}{x_3} \tag{36}$$

$$x_3 = \frac{D}{\frac{h1}{h_2} + \left(m+n-1\right)\frac{H}{h_2} + 1} \tag{37}$$

$$Rf_{mn} = \left(m+n-1\right)\sqrt{H^2 + {x_2}^2} + \sqrt{{h_1}^2 + x_1^2} + \sqrt{{h_2}^2 + x_3^2}\ . \tag{38}$$

For case 3 where $m = n$:

$$D = x_1 + x_2\left(m+n-1\right) + x_3 \tag{39}$$

$$\frac{H-h_1}{x_1} = \frac{H}{x_2} = \frac{h_2}{x_3} \tag{40}$$

$$x_3 = \frac{D}{\frac{H-h1}{h_2} + \left(m+n-1\right)\frac{H}{h_2} + 1} \tag{41}$$

$$Rf_{mn} = \left(m+n-1\right)\sqrt{H^2 + {x_2}^2} + \sqrt{\left(H-h_1\right)^2 + x_1^2} + \sqrt{{h_2}^2 + x_3^2}\ . \tag{42}$$

Finally, for case 4 where $m = n$:

$$D = x_1 + x_2\left(m+n-1\right) + x_3 \tag{43}$$

$$\frac{h_1}{x_1} = \frac{H}{x_2} = \frac{H-h_2}{x_3} \tag{44}$$

$$x_3 = \frac{D}{\frac{h1}{H-h_2} + \left(m+n-1\right)\frac{H}{H-h_2} + 1} \tag{45}$$

$$Rf_{mn} = \left(m+n-1\right)\sqrt{H^2 + {x_2}^2} + \sqrt{{h_1}^2 + x_1^2} + \sqrt{\left(H-h_2\right)^2 + x_3^2}\ . \tag{46}$$

These four sets of equations are used to compute the reflected path lengths between the transmitting antenna and observation point.

3. Geometrical Optics Waves Formulation

Electric fields generated from GO waves that bounce off of the ground plane and forest-air boundary back into the forest towards the observation point are defined by [14]:

$$E_{GO} = j\frac{\beta_f \eta_f I \Delta z}{4\pi} \cdot \frac{e^{-\alpha_f R f_{mn}} \cdot e^{-j\beta_f R f_{mn}} \left(\Gamma_f\right)^m \left(\Gamma_g\right)^n}{R f_{mn}} \tag{47}$$

where η_f is wave impedance of the forest layer, $I\Delta z$ is the source dipole moment where I is the current flowing through the dipole, and Δz is the length of dipole. We define Γ_f and Γ_g as the reflection coefficients for the forest-air and forest-ground boundaries, respectively.

4. Antenna Pattern Factor

The derivation of Eq. (47) does not take into account of the antenna pattern factor $\sin\theta$ illustrated in Figure 8. Overestimation of the electric field can occur when pattern factor is ignored. This overestimation of the electric field is only applicable for the V-pol for a vertically oriented dipole. The electric field for H-pol is omnidirectional and, thus, is independent of the $\sin\theta$ far-field pattern.

The far-field distance is dependent on the frequency of operation and the dimension of the antenna aperture. In order to determine the far-field distance, three conditions must be satisfied. The expressions for the three criteria are [33]:

$$R > \frac{2\Delta z^2}{\lambda} \tag{48}$$

$$R > 5\Delta z \tag{49}$$

$$R > 1.6\lambda \tag{50}$$

where R is the distance from dipole. All the units used for the quantities are in meters. Upon computation of each condition, we select the largest distance amongst the three values as R_{ff}. At distances greater than R_{ff} from transmitting antenna, the EM wave fronts are those of a spherical wave, which can be approximated locally as a plane wave.

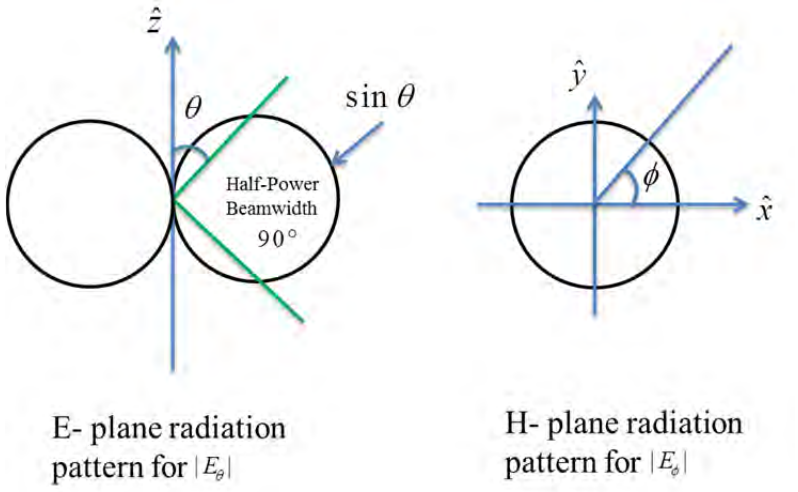

Figure 8. E - plane and H - plane radiation plots for an ideal dipole (after [33]).

The electric field in free space that is generated from an ideal dipole antenna is [33]:

$$\vec{E} = j\omega\mu \frac{I\Delta z}{4\pi} \cdot \frac{e^{-j\beta R}}{R} \sin\theta \ \hat{\theta} \tag{51}$$

where R is the distance from the dipole. The relation of the impedance of free space η_0 to the phase constant β is expressed as:

$$\eta_0 = \frac{\omega\mu}{\beta} \ . \tag{52}$$

The forest layer is a lossy medium; therefore, we replace the following terms $\omega\mu$, R, and $-j\beta$ in Eq. (51) with $\eta_f\beta_f$, Rf_{mn}, and $-\left(\alpha_f Rf_{mn} + j\beta_f Rf_{mn}\right)$, respectively. The expression for computing the electric field for the GO wave is:

$$E_{mn} = j\eta_f\beta_f \frac{I\Delta z}{4\pi} \left[\frac{e^{-\alpha_f Rf_{mn} - j\beta_f Rf_{mn}} \left(\Gamma_f\right)^m \left(\Gamma_g\right)^n}{Rf_{mn}} \right] \sin\theta \ . \tag{53}$$

The difference between Eq. (47) and Eq. (53) is evident. Firstly, there is an assumption made in Eq. (47) that the separation distance between the transmitting antenna and observation point is very large, making the angle θ close to $90°$. Thus, $\sin\theta \approx 1$. To illustrate the difference, we examine the case with the geometry depicted in

Figure 9. For simplification of the problem, we compute the electric fields of an ideal dipole in free space near a ground plane. A numerical computation based on Eq. (47) and Eq. (53) for vertical polarization is plotted in Figure 10.

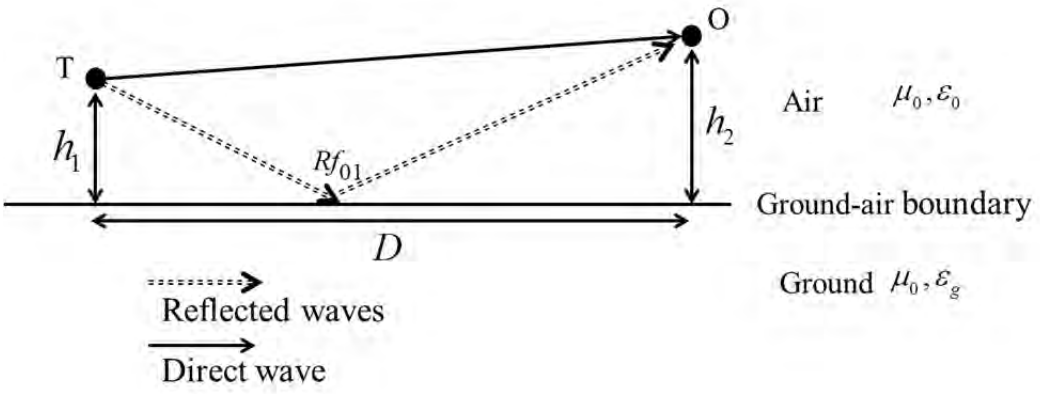

Figure 9. Geometry setup for antenna factor analysis.

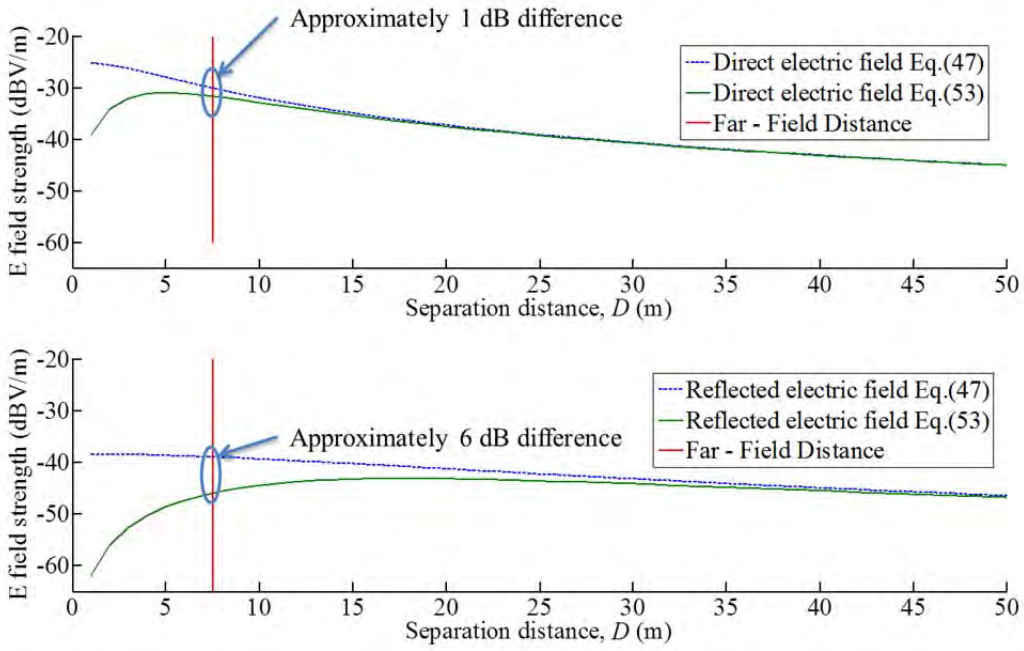

Figure 10. Effect of the antenna element factor on direct and reflected E field at 100 MHz.

From Figure 10, the impact of the antenna pattern on the electric field at near distances is greater for the reflected fields compared to the direct.

5. Lateral Wave Formulation

The components of the lateral wave appear in the form [12]:

$$E_z \cong E_L\left(\sqrt{\varepsilon_{f_c}-1}\cos\phi\cos\psi+\sin\psi\right) \tag{54}$$

$$E_\rho \cong E_L\left[\left(\varepsilon_{f_c}-1\right)\cos\phi\cos\psi+\left(\sqrt{\varepsilon_{f_c}-1}\right)\sin\psi\right] \tag{55}$$

$$E_\phi \cong E_L\sin\phi\cos\psi \tag{56}$$

where ψ is the inclination angle of the dipole antenna from horizontal in $\hat{x}-\hat{z}$ plane and ϕ is the angle from the $\hat{x}-\hat{z}$ plane. The term E_L used in Eqs. (54) – (56) is expressed as [12]:

$$E_L=\frac{60I\Delta z}{\varepsilon_{f_c}-1}\cdot\frac{e^{-j\beta\left(D+s\sqrt{\varepsilon_{f_c}-1}\right)}}{D^2} \tag{57}$$

where s is the total path length in the foliage between the transmitter and observation point. This path length is approximated as $s=2H-h_1-h_2$. The complex permittivity of the forest layer ε_{f_c} is defined in Eq. (15). As we are interested in computing the electric field of a wave propagating in the $\hat{x}-\hat{z}$ plane, only the terms E_z and E_ϕ are required. The E_z component from Eq. (54) is used for computing electric field for V-pol $\left(\phi=90°,\ \psi=0°\right)$, and E_ϕ from Eq. (56) is used in computing the electric field for H-pol $\left(\phi=0°,\ \psi=90°\right)$. The result is exactly the same as Eq. (57); therefore, the formula used to compute the lateral wave in this model is determined by Eq. (57) for both polarizations.

6. Transmission Loss Definition

The computation of the transmission loss TL_D in dB at a distance D in meters is defined as:

$$TL_D(dB) = 20\log_{10}\left|\vec{E}_D\right| - 20\log_{10}\left|\vec{E}_{1\text{ meter}}\right| \tag{58}$$

where $\left|\vec{E}_D\right|$ is the received field strength at the observation point at separation distance D and $\left|\vec{E}_{1\text{ meter}}\right|$ is the reference field strength at 1.0 m from transmitting antenna in free space without ground, as shown in Figure 12.

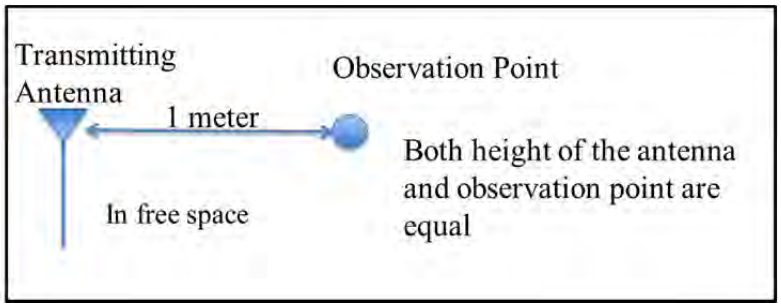

Figure 11. Reference electric field for computing the transmission loss.

In this chapter, we presented the three-layered model and a homogeneous model using the ray tracing method. The GO component and the lateral wave component are considered in the model. Modification of the GO equation was made to improve the near distance result by adding the antenna factor for V-pol. General equations were derived to compute the path length in foliage Rf_{mn}. The definition of transmission loss was given. Equation (57) is used to compute the lateral wave for both polarizations. In Chapter IV, the ray tracing model is validated by using the results generated by the model and by comparing those results with measured data.

IV. RESULTS AND ANALYSIS

In this chapter, we describe the two cases used to evaluate the ray tracing model. Results are discussed for each test case.

For Case I, measured data extracted from [14] is used. The simulation setup is done such that the height of the transmitting antenna remains at 3.96 m for all measurements, and the height of the observation point varies from 5.0 m to 28.96 m. Measured data were taken for both V-pol and H-pol at frequencies of 25 MHz, 50 MHz, and 100 MHz.

For Case II, we validate the ray tracing model using two empirical models mentioned in Chapter II (the JB model and Tewari's empirical model) together with measured data extracted from [7]. The 50 MHz data point from [7] is compared with the models. The root mean square (RMS) error δ_{RMS} in dB introduced in [31] is used to define a fitting value to quantify the performance of the ray tracing model with respect to measurements.

A. CASE I SETUP AND SIMULATION

Two sets of parameters are defined for this test setup. First is the geometry for the setup, which includes the physical heights of the forest, transmitting antenna, and observation point, and the separation distance. The geometry inputs for the setup are listed in Table 5.

Table 5. Geometrical inputs for Case I.

Parameter	Value	Units
Average Height of trees in forest layer, H	30.48	m
Separation Distance, D	1600	m
Height of transmitting antenna, h_1	3.96	m
For H-pol Height of observation point, h_2	5 – 29	m
For V-pol Height of observation point, h_2	7 – 29	m

The next set of input parameters are the electrical properties of each medium. The ground relative permittivity and ground conductivity listed in Table 6 is with reference to [14]. These values are typical ground values as reported in [20]. For the electrical properties of the forest media, we refer to Eq. (15) from Chapter II, where the forest layer's effective permittivity $\varepsilon_{f_r}\varepsilon_0$ and conductivity σ_f can be combined to form a complex permittivity.

The forest layer is modeled as an anisotropic medium in [14]. It has an effective permittivity and conductivity for the $\hat{z}$-direction as well as the tangential direction. The electrical properties of the $\hat{z}$-direction primarily affects the V-pol waves propagating in the forest layer. The electrical properties for the tangential direction primarily affect the H-pol waves propagating in the forest layer. The ray tracing model uses homogeneous media for all layers; thus, only the electrical properties corresponding to the polarization of interest are used as input. So for V-pol, the effective relative permittivity is represented by ε_{r_z} and conductivity by σ_z. The effective relative permittivity and conductivity for H-pol is represented by ε_{r_t} and σ_t, respectively. The initial values used in the simulation are the ones suggested in [14] and are listed in Table 6.

Table 6. Initial electrical properties of media for Case I.

Parameter	**Value**	**Units**
Frequency	25, 50, 100	MHz
Relative permittivity of air medium,	1	-
Conductivity of air medium	0	mS/m
Relative permittivity of ground medium	15	-
Conductivity of ground medium	10	mS/m
Relative permittivity of forest medium (V-pol)	1.0530	-
Conductivity of forest medium (V-pol)	0.1180	mS/m
Relative permittivity of forest medium (H-pol)	1.0080	-
Conductivity of forest medium (H-pol)	0.0300	mS/m

Upon establishing all the necessary values for Case I, an iterative process is performed to obtain the modified effective parameters that give the best agreement between the simulated and measured data. The process consists of two steps. Firstly, the

relative permittivity of the forest layer is fixed at a constant value while changing the value of conductivity of the forest media. The initial constant value of relative permittivity for the forest layer used is with reference to optimized data in [14]. Upon getting a minimum average error value, the relative permittivity value is then tuned to achieve lowest possible average error.

1. Case I Results

The final adjusted relative effective permittivity ε_{r_z} and conductivity σ_z corresponding to the $\hat{z}$-direction are tabulated in Table 7 at three frequency points (25 MHz, 50 MHz, and 100 MHz). Similarly in Table 8, the final adjusted relative effective permittivity ε_{r_t} and conductivity σ_t that correspond to the tangential direction are tabulated.

The simulated loss versus height curves for frequencies of 25 MHz, 50 MHz, and 100 MHz for V-pol are plotted in Figure 12 to Figure 14, respectively. Similarly, the simulated loss curves for the same frequency points for H-pol are plotted in Figure 15 to Figure 17, respectively. In both cases, measured data points are superimposed on the simulated results.

Table 7. Effective permittivity and conductivity for the ray tracing method and Sommerfeld solution from [14] (V-pol).

V-pol	**Sommerfeld solution**		**Ray tracing model**	
Frequency (MHz)	ε_{r_z}	σ_z (mS/m)	ε_{r_z}	σ_z (mS/m)
25	1.0530	0.1180	1.0600	0.1010
50	1.0180	0.0730	1.0400	0.0930
100	1.0060	0.0420	1.0250	0.0760

Table 8. Effective permittivity and conductivity for the ray tracing method and Sommerfeld solution from [14] (H-pol).

H-pol	Sommerfeld solution		Ray tracing model	
Frequency (MHz)	ε_{r_t}	σ_t (mS/m)	ε_{r_t}	σ_t (mS/m)
25	1.0080	0.0300	1.0090	0.0300
50	1.0100	0.0370	1.0110	0.0410
100	1.0100	0.0420	1.0610	0.0550

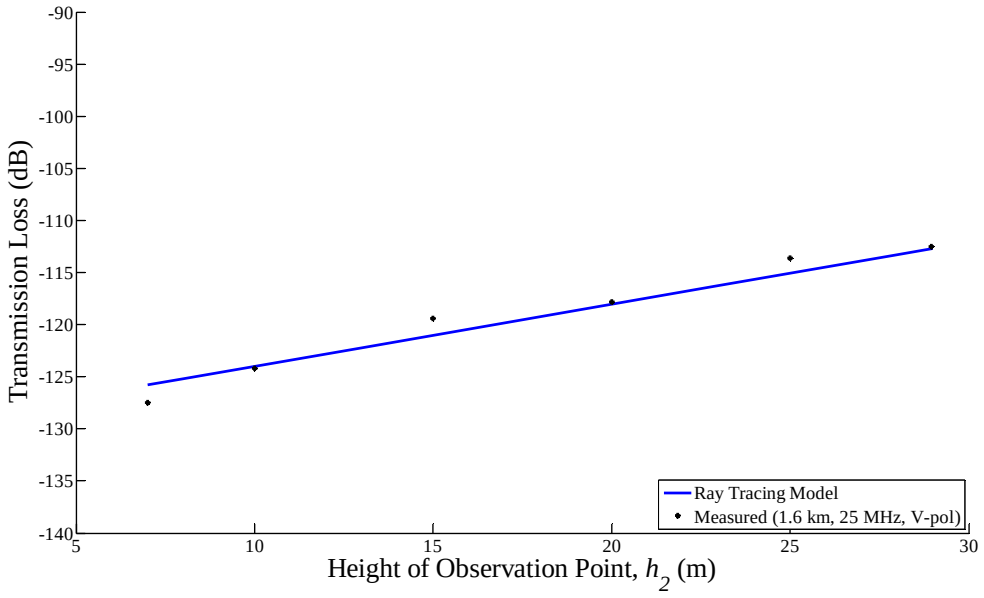

Figure 12. Measured data from [14] versus ray tracing model (1.6 km, 25 MHz, V-pol).

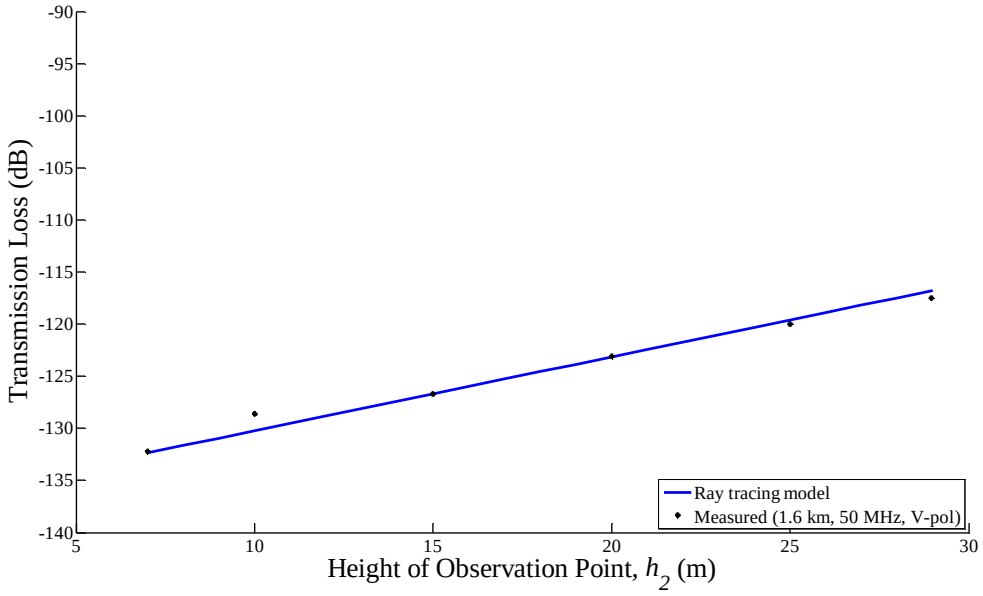

Figure 13. Measured data from [14] versus ray tracing model (1.6 km, 50 MHz, V-pol).

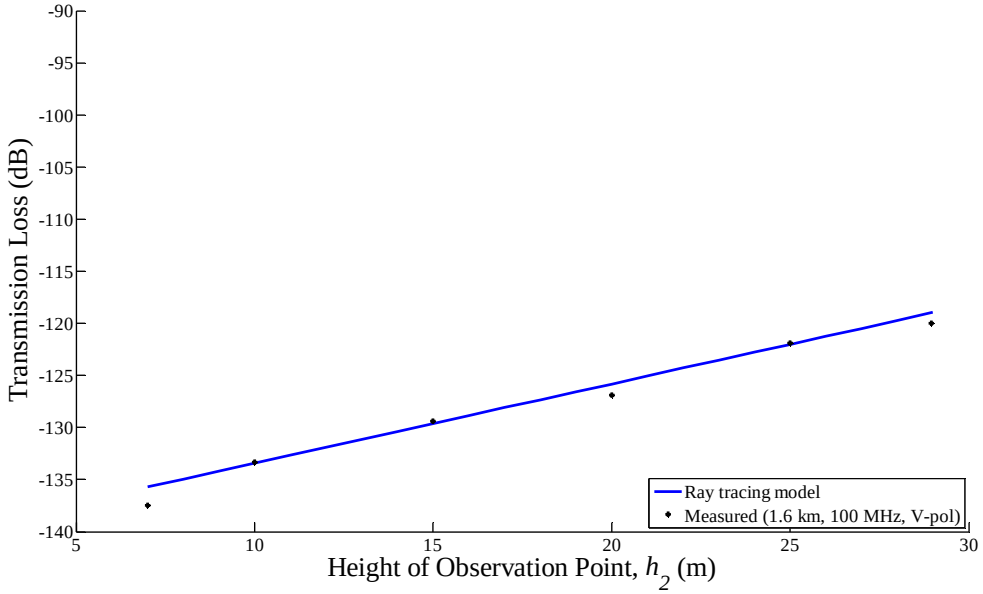

Figure 14. Measured data from [14] versus ray tracing model (1.6 km, 100 MHz, V-pol).

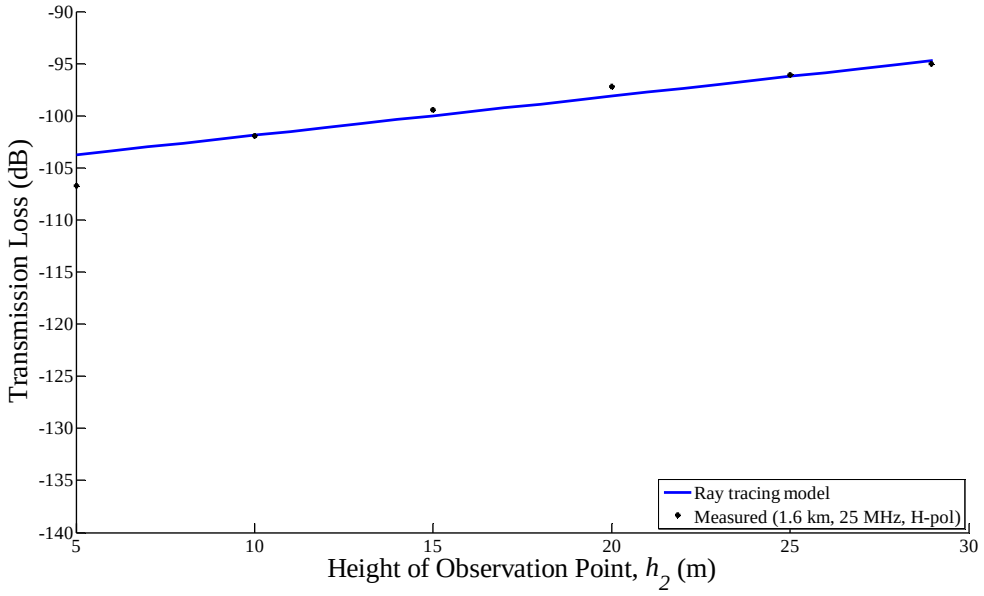

Figure 15. Measured data from [14] versus ray tracing model (1.6 km, 25 MHz, H-pol).

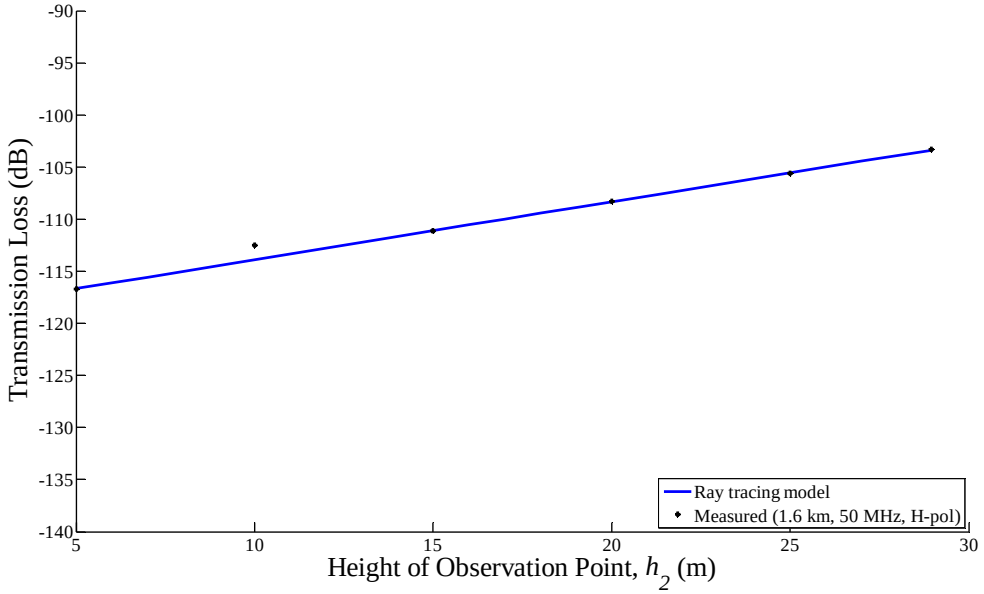

Figure 16. Measured data from [14] versus ray tracing model (1.6 km, 50 MHz, H-pol).

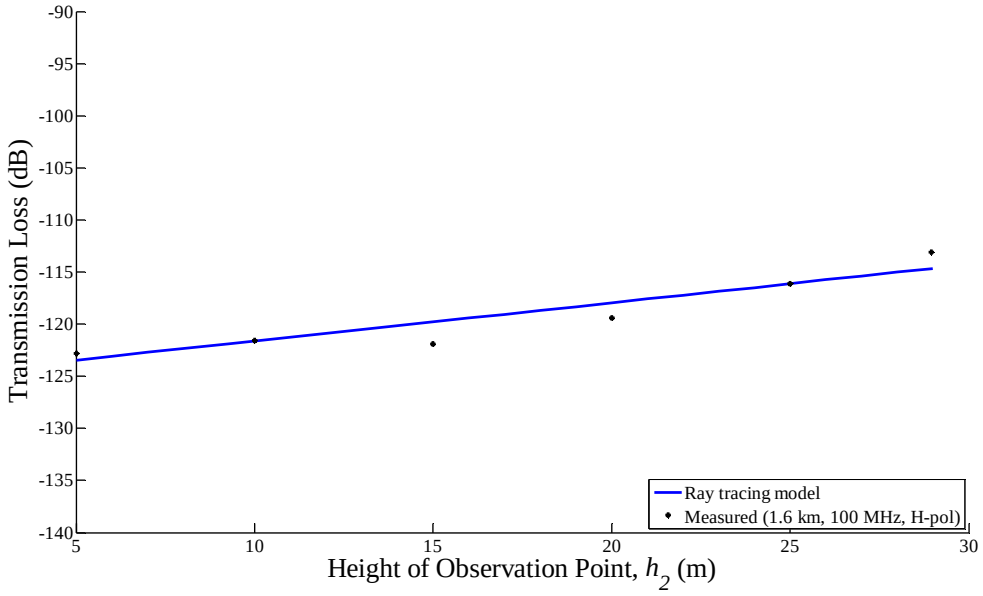

Figure 17. Measured data from [14] versus ray tracing model (1.6 km, 100 MHz, H-pol).

2. Case I Analysis and Comments

The results generated by the ray tracing model were based on the assumption that forest media is isotropic and homogenous. The average difference between each measured data point with the simulated data point at each frequency is tabulated in Table 9. The difference for both polarizations was within $\pm$ 1 dB, similar to that of the Sommerfeld solution [14]. The idea of using a homogenous medium to represent the forest layer provided a satisfactory correlation to the measured data (within 1 dB) up to a frequency of 100 MHz. Another observation was the reduction of loss with increase in height of observation point. This is expected because the path length in the lossy foliage decreases as the antenna height increases.

Table 9. Average error between measured data from [14] and ray tracing model with adjusted parameter.

	Average error compared between model and measured data (dB)			
	H-pol to H-pol		**V-pol to V-pol**	
Frequency (MHz)	Sommerfeld solution	Ray Tracing Model	Sommerfeld solution	Ray Tracing Model
25	0.60	0.82	0.30	0.90
50	0.80	0.23	0.40	0.48
100	0.90	0.97	0.40	0.72

Up to this point, the model was validated to 100 MHz at a separation distance of 1.6 km. Further testing is needed to validate the range applicability of the ray tracing model.

B. CASE II SETUP AND SIMULATION

In Case I, we commented that the ray tracing model was able to provide satisfactory estimation of the transmission loss at a fixed separation distance of up to 100 MHz. Further verification on the applicability of the ray tracing model was made by comparing it with another set of measured data collected for the northern part of India from [7]. Procedures established in Case I were repeated, where we defined the geometry inputs (refer to Table 10) and the estimated electrical properties of each medium (refer to Table 11). For Case II, the electrical properties of the forest were taken from the measured data via the inverse method as documented in [26].

Table 10. Geometrical inputs for Case II.

Parameter	**Value**	**Units**
Average Height of trees in forest layer, H	20	m
Separation Distance, D	1–4200	m
Height of transmitting antenna, h_1	5	m
Height of observation point, h_2 (For H-pol or V-pol)	5	m

Table 11. Electrical properties of each medium for Case II.

Parameter	Value	Units
Frequency	50	MHz
Relative permittivity of air medium,	1	-
Conductivity of air medium	0	mS/m
Relative permittivity of ground medium	15	-
Conductivity of ground medium	10	mS/m
Relative permittivity of forest medium	1.065	-
Conductivity of forest medium	0.135	mS/m

1. Case II Results

In conjunction with the measured data used [7], two empirical models were used for comparison. The data are plotted in Figure 18 and Figure 19.

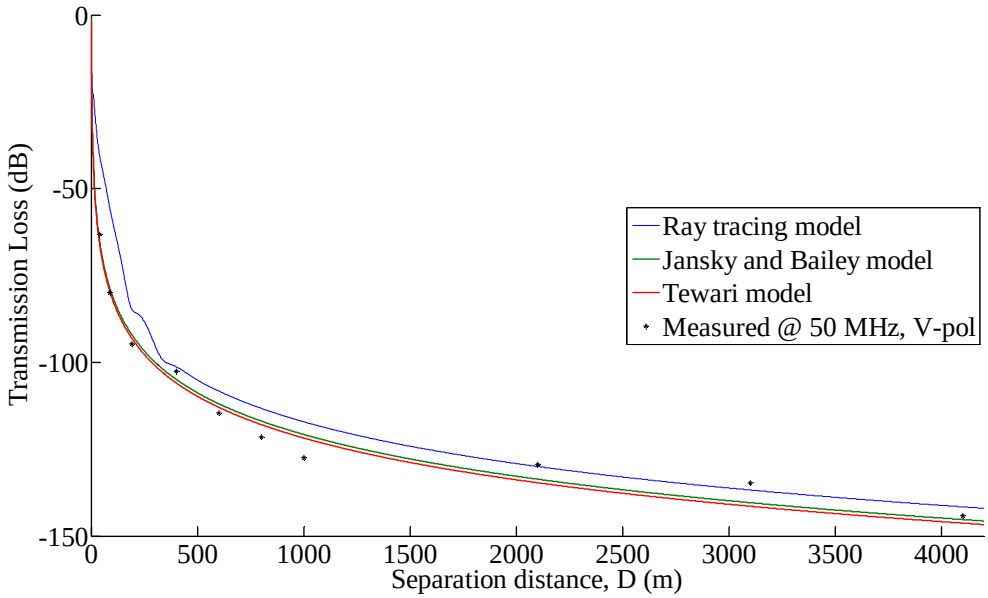

Figure 18. Measured data from [7] versus predictions from models at 50 MHz, V-pol.

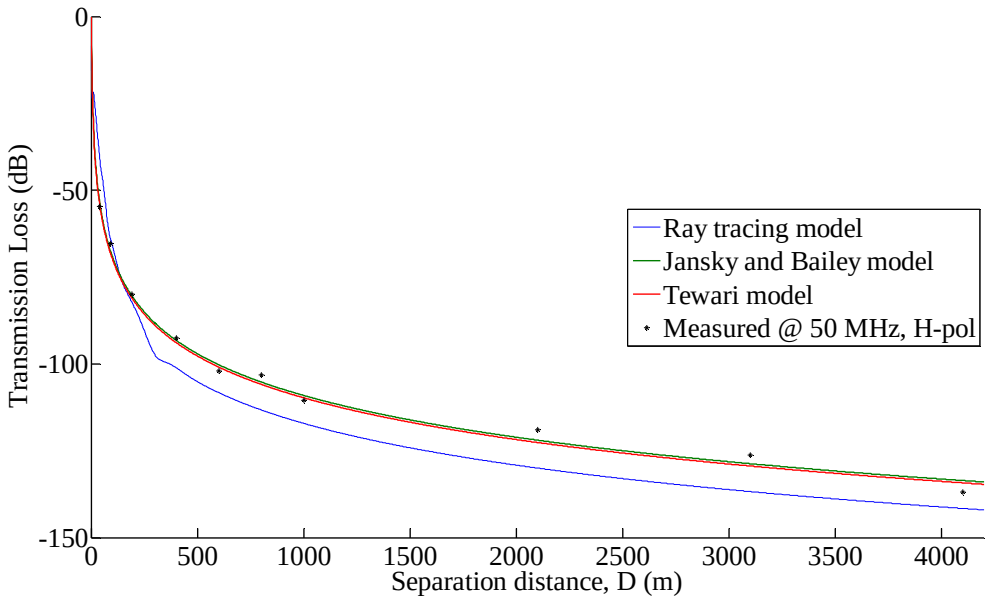

Figure 19. Measured data from [7] versus prediction from models at 50 MHz, H-pol.

A useful quantity to compare the performance of the models is needed. A good figure of merit is the RMS error defined in [31]:

$$\delta_{RMS}(dB) = \sqrt{\frac{\sum_{i=1}^{N}\left(E_i^2\right)}{N}} \tag{59}$$

where δ_{RMS} is the RMS error in dB, N is number of measured data points, and E_i is the absolute difference in dB between the measured and the simulated data. The RMS errors for both polarizations at 50 MHz are tabulated in Table 12.

Table 12. RMS error at 50 MHz.

Polarization	**Ray Tracing Model, δ_{RMS} (dB)**	**Tewari's Empirical Model, δ_{RMS} (dB)**	**JB Empirical Model, δ_{RMS} (dB)**
V-pol	3.7685	1.1873	1.2047
H-pol	2.6869	0.6528	0.7097

2. Case II Analysis and Comments

The RMS error value of the ray tracing model was much higher compared to the other two empirical models. From [12], it was suggested that the formulation for the transmission loss only applies for separation distance D greater than 1.0 km. To investigate this, we considered only measured data points where separation distance D was larger than 1.0 km. A new computation of the RMS error was performed and the results tabulated in Table 13.

Table 13. RMS error at 50 MHz with D greater than 1.0 km.

Polarization	**Ray Tracing Model, δ_{RMS} (dB)**	**Tewari's Empirical Model, δ_{RMS} (dB)**	**JB Empirical Model, δ_{RMS} (dB)**
V-pol	2.7073	2.4377	2.5979
H-pol	4.3222	1.3141	1.3813

RMS error for V-pol is reduced and closer to both empirical models when the simulated data are compared to measured data at separation distance D greater than 1.0 km; however, we still observe large differences for H-pol. This could be due to two possible reasons. First, in the formulation of the lateral wave equation, both the polarizations use the same expressions. Second, the electrical properties for both V-pol and H-pol are of the same values with reference to Table 2. Based on findings in [14], a higher forest conductivity σ_f value for V-pol is used compared to the H-pol. This is explained by stronger scattering of the vertical polarized electric fields due to the vertical tree trunks in the forest layer [14]. To further investigate this characteristic, the forest conductivity was reduced by 30 percent from 0.135 mS/m to 0.095 mS/m. The new resultant RMS error for the ray tracing model is tabulated in Table 14.

Table 14. RMS error with D greater than 1.0 km and lower forest conductivity.

Polarization	**Ray Tracing Model, δ_{RMS} (dB)**	**Tewari's Empirical Model, δ_{RMS} (dB)**	**JB Empirical Model, δ_{RMS} (dB)**
H-pol	1.3415	1.3141	1.3813

The new resultant RMS error based on the new forest conductivity is reduced. This constitutes a smaller difference between the other two empirical models at a separation distance greater than 1.0 km. This finding suggests that higher attenuation is experienced by the vertical polarized electric field compared to horizontal polarized electric fields when propagating within the forest media; however, this reduction in forest conductivity should not be taken as a proportional effect compared to the scattering effects from the tree trunks. It only means that for estimation of transmission loss within a forest media, the attenuation by the V-pol electric field is in general greater than that of the H-pol electric field.

V. CONCLUSIONS AND RECOMMENDATIONS

A. SUMMARY

A ray tracing model, based on the three-layer planar stratified medium shown in Figure 2, was coded in MATLAB. It allows users to numerically compute the electric field and to analyze direct waves, multiple reflected waves, and lateral waves or a summation of all of these components

For the formulation to compute the electric field for reflected and direct rays, an antenna pattern factor was introduced [14]. It was found that V-pol reflected waves are affected more by the factor $\sin\theta$ compared to the direct waves. The antenna pattern factor is not applicable to the H-pol electric fields as the antenna pattern is omnidirectional. A set of equations was introduced to compute the multi-bounce path lengths within the foliage. These equations were derived by applying the well-known Snell's law of reflection [27] as well as the properties of symmetrical triangles where the all sides of each triangle are proportional. For the computation of the lateral waves, the equation derived in [12] was used and is applicable for both V-pol and H-pol.

The ray tracing model was compared to measured data for two cases. In Case I, simulated results at 25 MHz, 50 MHz, and 100 MHz for both H-pol and V-pol were compared to the measured results reported in [14]. Results suggested that the homogeneous media representing the forest layer was applicable up to 100 MHz and at a separation distance of 1.6 km. This upper frequency limit of the ray tracing model was consistent with the applicable frequency reported in [12]. In Case II, another comparison was performed to determine the useful range of the model. A comparison at 50 MHz was made with two other empirical models (JB model and Tewari's empirical model) together with measured data approximated from [7]. To quantify the performance, a RMS error defined in [31] was introduced. The RMS error of the ray tracing model for V-pol at 50 MHz showed good agreement with two other empirical models (the JB model and the Tewari's empirical model) at separation distances beyond 1.0 km. For the H-pol at the same frequency, we observed large differences in the RMS error between the ray tracing

model and the other two empirical models. This was explained by the scattering effect of the tree trunks. It was found that the V-pol electric fields experienced more attenuation compared to the H-pol electric fields due to the greater scattering effect caused by the physical vertical tree trunks within the forest [14]. This was confirmed by tuning the conductivity of the forest media to a lower value that corresponds to lower transmission loss.

B. CONCLUSION

In conclusion, a physics-based model provides a fundamental knowledge of wave propagation in stratified media useful for further research purposes. A propagation loss prediction model using the ray tracing method was successfully implemented for Configuration 2 in Figure 3. Leveraging on the previous works done by Tamir [18] and Li [14], we were able to formulate the model for applications where communication devices are operating at a frequency less than 100 MHz, with the minimum distance between the communication devices being at least 1.0 km apart within a forest environment. This ray tracing model used the three-layer planar stratified medium shown in Figure 2 and was coded using MATLAB software. It allows users to compute the electric field for direct waves, multiple reflected waves, and lateral waves or a summation of all these waves within the forest medium numerically. Through the use of analytical methods, the geometry of the problem can be extended to greater depth of the forest compared to the CEM used in previous work [13], where the computational resources and time needed are greater.

In Case II, it was suggested that vertical electric fields propagating within the forest medium in general experience more scattering effects due to the vertical tree trunks; therefore, higher attenuations occur compared to the horizontal polarized electric fields [14].

C. RECOMMENDATIONS

During the course of analyzing the simulated transmission loss in Case I, the effective parameters of the forest layer used from [14] played an important role. These values served as an initial input parameter and were subsequently tuned during the iterative process to match the measured data. There is a need to determine these effective parameters either via empirical models or via measurements when no initial input parameters are provided.

The work done in this thesis serves as an initial platform that allows further modification of the formulation to support other types of configurations depicted in Figure 3. This is essentially useful for different types of communication systems deployed in various scenarios that can be similar to the possible configurations mentioned. The formulation of the model could reference Tamir's ray tracing method in [18].

Another limitation of the model that requires further improvement is short range transmission loss prediction. From Case I and Case II, the model is applicable in predicting transmission loss for communication links greater than 1 km. One possible software tool for modeling of the short range propagation loss at VHF band is CST Microwave Studio. This overcomes the limitation of the existing model; but the simulation time can be extremely long (days).

THIS PAGE INTENTIONALLY LEFT BLANK

APPENDIX A. SOFTWARE DESCRIPTION

The ray tracing model is coded using the MATLAB program and inputs are keyed into the script window before running the codes. There are several inputs required from the user, such as the dimensions of the forest in terms of depth and average height of the forest layer. The list of parameters is populated in Table 15.

Table 15. Input parameters for the ray tracing model.

Description	Symbol used in MATLAB code	Units
Average Height of the forest layer	H	m
Height of transmitting antenna	h1	m
Height of observation point	h2	m
Separation Distance	D	m
Frequency	fMHz	MHz
Polarization (V-pol, H-pol)	POLAR_Sel	-
Effective relative permittivity of forest layer	ef	-
Effective relative permittivity of ground layer	eg	-
Effective relative permittivity of air layer	ea	-
Conductivity of forest layer	sigma1	S/m
Conductivity of ground layer	sigma2	S/m
Conductivity of air layer	sigma3	S/m
Current flowing through dipole	I	A
Length of dipole	deltaZ	m

The overview of the ray tracing model coded in MATLAB is illustrated in Figure 20.

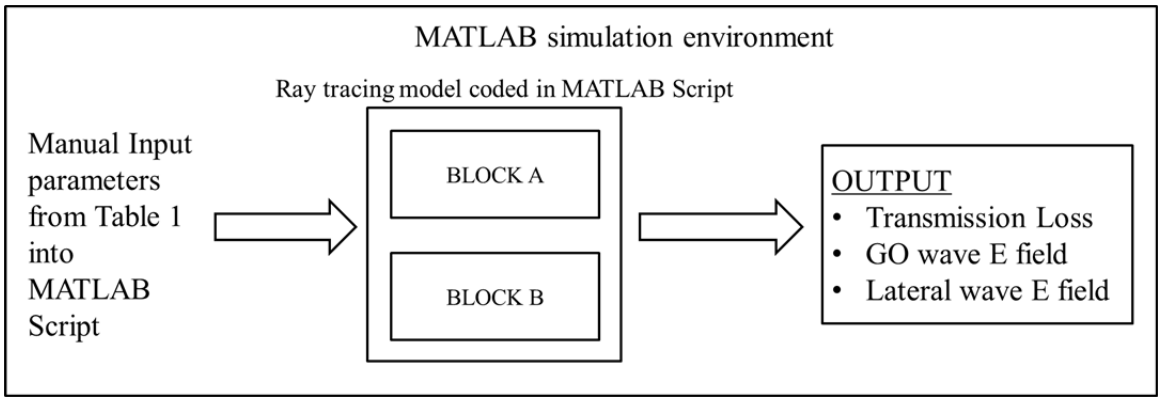

Figure 20. Overview of ray tracing model in MATLAB simulation environment

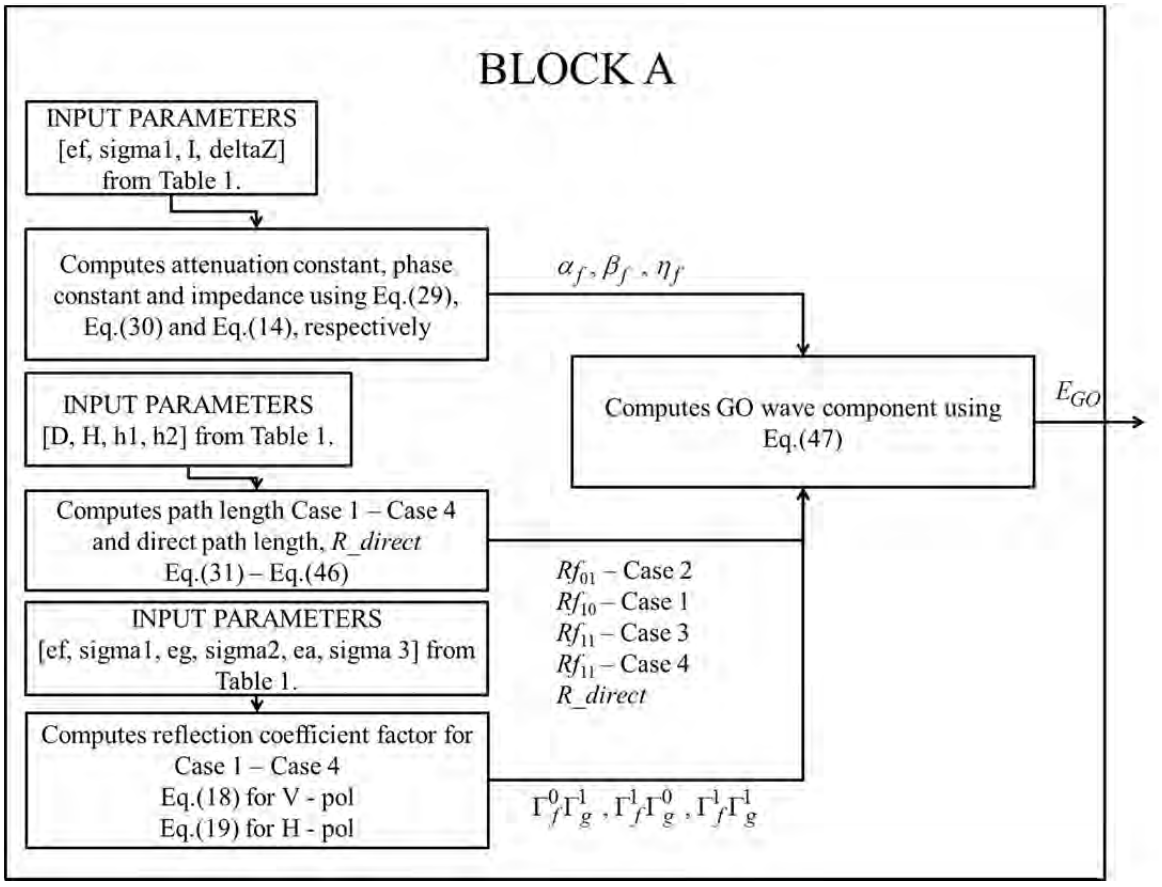

Figure 21. Generic flow diagram within Block A.

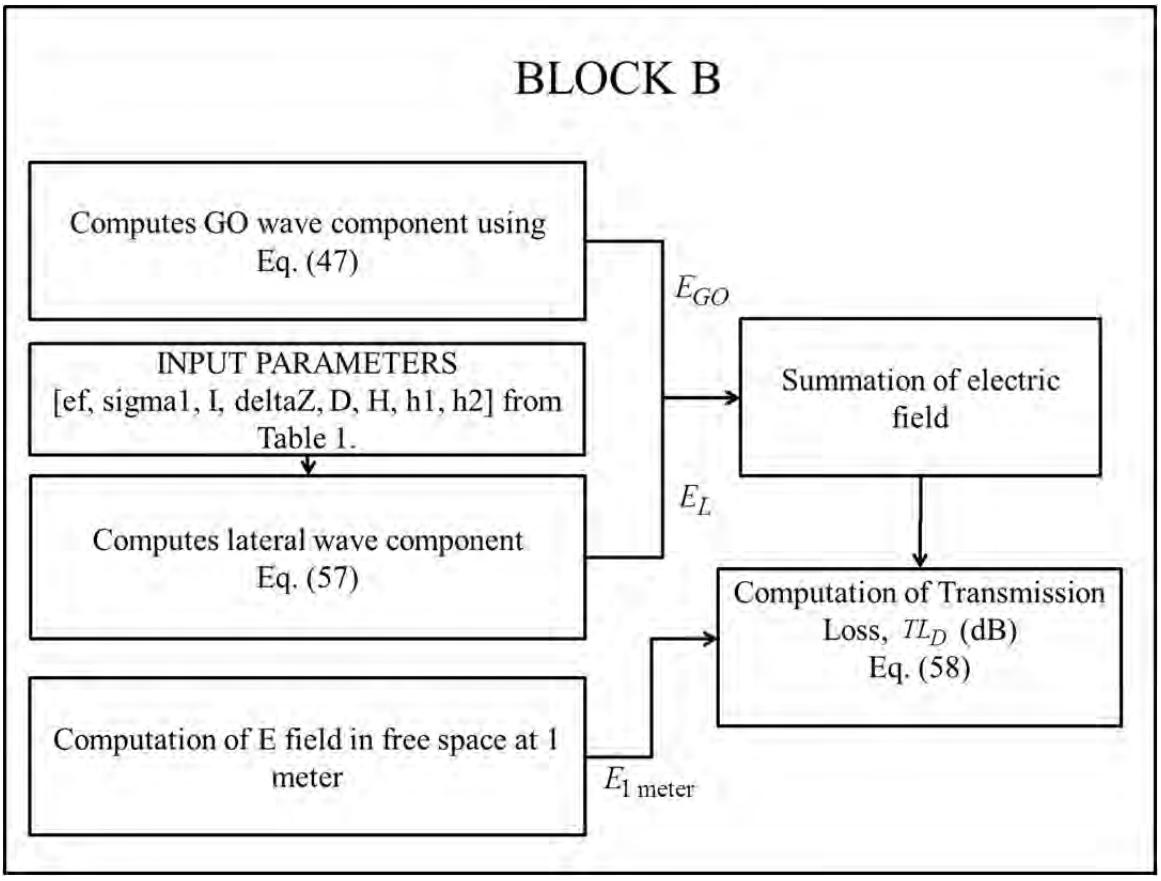

Figure 22. Generic flow diagram within Block B.

The ray tracing model was coded in MATLAB that allows user to decide and code their preferred output for analysis. In this thesis, computation of transmission loss over different observation height was coded for Case I. For Case II, the transmission loss over separation distance was computed.

THIS PAGE INTENTIONALLY LEFT BLANK

APPENDIX B. ABSOLUTE DIFFERENCE DATA FOR CASE I

Table 16. Absolute difference (dB) between ray tracing model and measured data at 25 MHz (V-pol).

Height of Observation Point, h_2 (m)	TL_D (dB) at 25 MHz from [14]	Ray Tracing Model (dB)	Absolute difference (dB)
5	-127.5	-125.8	1.7
10	-124.2	-124.0	0.2
15	-119.4	-121.0	1.6
20	-117.8	-118.0	0.2
25	-113.6	-115.1	1.5
28.96	-112.5	-112.7	0.2

Table 17. Absolute difference (dB) between ray tracing model and measured data at 50 MHz (V-pol).

Height of Observation Point, h_2 (m)	TL_D (dB) at 50 MHz from [14]	Ray Tracing Model (dB)	Absolute difference (dB)
5	-132.2	-132.4	0.2
10	-128.6	-130.2	1.6
15	-126.7	.126.7	0.0
20	-123.1	-123.1	0.0
25	-120.0	-119.6	0.4
28.96	-117.5	-116.8	0.7

Table 18. Absolute difference (dB) between ray tracing model and measured data at 100 MHz (V-pol).

Height of Observation Point, h_2 (m)	TL_D (dB) at 100 MHz from [14]	Ray Tracing Model (dB)	Absolute difference (dB)
5	-137.5	-135.7	1.8
10	-133.3	-133.4	0.1
15	-129.4	-129.6	0.2
20	-126.9	-125.8	1.1
25	-121.9	-122.0	0.1
28.96	-120.0	-119.0	1.0

Table 19. Absolute difference (dB) between ray tracing model and measured data at 25 MHz (H-pol).

Height of Observation Point, h_2 (m)	**TL_D (dB) at 25 MHz from [14]**	**Ray Tracing Model (dB)**	**Absolute difference (dB)**
5	-106.7	-103.7	3.0
10	-101.9	-101.9	0.0
15	-99.4	-100.0	0.6
20	-97.2	-98.1	0.9
25	-96.1	-96.2	0.1
28.96	-95.0	-94.7	0.3

Table 20. Absolute difference (dB) between ray tracing model and measured data at 50 MHz (H-pol).

Height of Observation Point, h_2 (m)	**TL_D (dB) at 50 MHz from [14]**	**Ray Tracing Model (dB)**	**Absolute difference (dB)**
5	-116.7	-116.7	0.0
10	-112.5	-113.9	1.4
15	-111.1	-111.1	0.0
20	-108.3	-108.3	0.0
25	-105.6	-105.6	0.0
28.96	-103.3	-103.3	0.0

Table 21. Absolute difference (dB) between ray tracing model and measured data at 100 MHz (H-pol).

Height of Observation Point, h_2 (m)	**TL_D (dB) at 100 MHz from [14]**	**Ray Tracing Model (dB)**	**Absolute difference (dB)**
5	-122.8	-12.5	0.7
10	-121.6	-121.6	0.0
15	-121.9	-119.8	2.1
20	-119.4	-118.0	1.4
25	-116.1	-116.1	0.0
28.96	-113.1	-114.7	1.6

APPENDIX C. ABSOLUTE DIFFERENCE DATA FOR CASE II

Table 22. Absolute difference (dB) between ray tracing model and measured data at 50 MHz (V-pol).

Separation Distance, D (m)	**TL_D (dB) at 50 MHz from [7]**	**Ray Tracing Model (dB)**	**Absolute difference, E_i (dB)**
40	-63.2	-40.4	22.8
90	-80.0	-56.1	23.9
192	-94.7	-84.8	9.9
400	-102.6	-101.2	1.4
600	-114.7	-108.2	6.5
800	-121.6	-113.2	8.4
1000	-127.4	-117.1	10.3
2100	-129.5	-130.0	0.5
3100	-134.7	-136.8	2.1
4100	-144.2	-141.6	2.6

Table 23. Absolute difference (dB) between ray tracing model and measured data at 50 MHz (H-pol).

Separation Distance, D (m)	**TL_D (dB) at 50 MHz from [7]**	**Ray Tracing Model (dB)**	**Absolute difference, E_i (dB)**
40	-54.7	-40.3	14.4
91	-65.3	-63.9	1.4
192	-80.0	-82.2	2.2
400	-92.6	-101.0	8.4
600	-102.1	-108.2	6.1
800	-103.2	-113.2	10.0
1000	-110.5	-117.1	6.6
2100	-118.9	-130.0	11.1
3100	-126.3	-136.8	10.5
4100	-136.8	-141.6	4.8

THIS PAGE INTENTIONALLY LEFT BLANK

LIST OF REFERENCES

[1] Y. S. Meng, Y. H. Lee, and B. C. Ng, "Study of propagation loss prediction in forest environment," *Progress in Electromagn. Res. B*, vol. 17, pp. 117–133, 2009.

[2] L. W. Li, T. S. Yeo, P. S. Kooi, and M. S. Leong, "Radiowave propagation along mixed paths through a four-layered model of rain forest: an analytic approach," *IEEE Trans. on Antennas Propagat.*, vol. 46, no. 7, pp. 1098–1111, 1998.

[3] L. o. t. Internet, "Learn on the Internet." [Online]. Accessed August 4, 2014. Available: http://www.geography.learnontheinternet.co.uk /images/ecosystems/crosssection1.gif

[4] G. G. Joshi, C. B. Dietrich Jr., C. R. Anderson, W. G. Newhall, W. A. Davis, J. Isaacs, and G. Barnett, "Near ground channel measurements over line of sight and forested paths," *IEEE Proc. in Microw., Antennas Propag.*, vol. 152, no. 6, pp. 589–596, 2005.

[5] M. S. Assis, "Search and rescue in forest environment," in *Microwave and Optoelectronics Conference SBMO/IEEE MTT-S International*, Belem, Brazil, 2009.

[6] K. Phaebua, C. Phongcharoenpanich, M. Krairiksh, and T. Lertwiriyaprapa, "Path loss prediction of radiowave propagation in an orchard by using modified UTD method," *Progress in Electromag. Res.*, vol. 239, pp. 347–363, 2012.

[7] R. K. Tewari, S. Swarup and N. R. Manujendra, "Radiowave propagation through rain forests of India," *IEEE Trans. on Antennas Propag.*, vol. 38, no. 4, pp. 433–449, 1990.

[8] J. J. Hicks, A. P. Murphy, E. L. Patrick, and L. G. Sturgill, "Tropical propagation research final report Volume II," Atlantic Research Corporation, Alexandria, VA , 1970.

[9] CCIR, "Influences of terrain irregularities and vegetation on troposphere propagation," CCIR Report, pp. 235–236, Geneva, Switzerland, 1986.

[10] M. A. Weissberger, "An initial critical summary of models for predicting the attenuation of radiowaves by trees," Electromagnetic Compatibility Analysis Center, Annapolis, MD, 1982.

[11] COST235, "Radio propagation effects on next-generation fixed-service terrestrial telecommunication systems," Final Report, Luxembourg, 1996.

[12] T. Tamir, “On radiowave propagation in forest environments,” *IEEE Trans. on Antennas Propag.*, vol. AP-15, no. 6, pp. 806–817, November 1967.

[13] C. W. Chan, “Investigation of propagation in foliage using simulation techniques,” M.S. thesis, Department of Electrical and Computer Engineering, Naval Postgraduate School, Monterey, CA, September 2011.

[14] Y. Li and H. Ling, “Numerical modeling and mechanism analysis of VHF wave propagation in forested environments using the equivalent slab model,” *Progress in Electromag. Res.*, vol. 91, pp. 17–34, 2009.

[15] S. S. Seker and A. Schneider, “Stochastic model for pulsed radio transmission through stratified forests,” in *IEEE Proc. Microw., Antennas Propag.*, vol. 134, no. 4, pp. 361–368, 1987.

[16] D. Liao and K. Sarabandi, “Modeling and simulation of near earth propagation in presence of a truncated vegetation layer,” *IEEE Trans. on Antennas Propag.*, vol. 55, no. 3, pp. 949–957, 2007.

[17] D. Liao and K. Sarabandi, “Near earth wave propagation characteristics of electric dipole in presence of vegetation or snow layer,” *IEEE Trans. on Antennas Propag.*, vol. 53, no. 11, pp. 3747–3756, 2005.

[18] T. Tamir, “Radiowave propagation along mixed paths in forest environments,” *IEEE Trans. on Antennas Propag.*, vols. AP-25, no. 4, pp. 471–477, 1977.

[19] J. H. Koh, L. W. Li, P. S. Kooi, T. S. Yeo, and M. S. Leong , “Dominant lateral waves in canopy layer of a four-layered forest,” in *Asia Pacific Microwave Conf.*, Hong Kong, 1997.

[20] D. Dence and T. Tamir, “Radio loss of lateral waves in forest environments,” *Radio Sci.*, vol. 4, no. 4, pp. 307–318, 1969.

[21] M. Le Palud, “Propagation modeling of VHF radio channel in forest environments,” in *IEEE Military Commun. Conf.*, Monterey, CA, 2004.

[22] G. Cavalcante and A. Giarola, “Optimization of Radio Communication in Media with Three layers,” *IEEE Trans. on Antennas Propag.*, vol. AP-31, no. 1, pp. 141–145, 1983.

[23] G. Cavalcante, D. Rogers and A. Giarola, “Radio loss in forests using a model with four layered media,” *Radio Sci.*, vol. 18, no. 5, pp. 691–695, 1983.

[24] S. S. Seker, “Radio pulse transmission along mixed paths in a stratified forest,” *IEEE Proc. Microw., Antennas Propag.*, vol. 136, no. 1, pp. 13–18, 1989.

[25] J. H. Koh, L. W. Li, P. S. Kooi, T. S. Yeo, and M. S. Leong, “Dominant lateral waves in the canopy layer of a four-layered forest,” *Radio Sci.*, vol. 34, no. 3, pp. 681–691, 1999.

[26] R. K. Tewari, S. Swarup, and M. N. Roy, “Evaluation of relative permitivity and conductivity of forest slab from experimentally measured data on lateral wave attenuation constant,” *Int. J. of Electron.*, vol. 61, no. 5, pp. 597–605, 1986.

[27] D. M. Pozar, *Microwave Engineering*, Hoboken, NJ: John Wiley & Sons, 2005, pp. 1–48.

[28] H. W. Parker and G. H. Hagn, “Feasibility study of the use of open wire transmission lines, capacitors and cavities to measure the electrical properties of vegetation,” Standford Research Institute, Menlo Park, CA, 1966.

[29] J. J. Holmes and C. A. Balanis, “Refraction of a uniform plane wave incident on a plane boundary between two lossy media,” *IEEE Trans. on Antennas Propag.*, vol. AP-26, no. 5, pp. 738–741, 1978.

[30] S. T. Rapport, *Wireless Communications Principles and Practice,* 2nd ed. Upper Saddle River, NJ: Prentice Hall, 2002.

[31] M. O. Al-Nuaimi and R. Stephens, “Measurements and prediction model optimization for signal attenuation in vegetation media at centimetre wave frequencies,” *Proc. in Microw., Antennas Propag.*, vol. 145, no. 3, pp. 201–206, 1998.

[32] Y. S. Meng, Y. H. Lee, and B. C. Ng, “Empirical near ground path loss modeling in a forest at VHF and UHF,” *IEEE Trans. on Antennas Propag.*, vol. 57, no. 5, pp. 1461–1468, 2009.

[33] W. L. Stutzman and G. A. Thiele, *Antenna Theory and Design*, Hoboken, NJ: John Wiley & Sons, 2013, pp. 32–40.

THIS PAGE INTENTIONALLY LEFT BLANK

INITIAL DISTRIBUTION LIST

1. Defense Technical Information Center
   Ft. Belvoir, Virginia

2. Dudley Knox Library
   Naval Postgraduate School
   Monterey, California